MASTER THESIS

Data Analysis for Citizen-science Cosmic Ray Muon Detector

Priyanka Kesavadas

Matrikel Number 66129

Supervisor: ***Prof. Dr. Michael Schmelling***

Referee: ***Prof. Dr. rer. nat. Michael Bantel***

Co-Referee: ***Prof. Dr. techn. Herman-Jalli Ng***

Master Thesis Number: 530

Duration: 15 January 2020 till 15 August 2020

15 August 2020

Abstract

Muons found in secondary cosmic rays are elementary particles created by high energy collisions of extra-terrestrial particles with the earth's upper atmosphere. The focus of this thesis is to analyse test data from two pairs of prototype detector boards, which detect such muons. This allows characterization of the performance of the system under various operating conditions, and to determine the optimum design for citizen science cosmic ray studies so as to better understand the muon detector and improve the performance thereby enhancing detection. The results are obtained by running the PIN-diode detectors together with a high-efficiency scintillator counter that serves as a reference.

Declaration

I hereby certify that this thesis is based on my own work which is a result of my personal study and experiments done within the LHCb group of the Max-Planck-Institut für Kernphysik, Heidelberg under the supervision of ***Prof. Michael Schmelling*** and in collaboration with ***Prof. Dr. rer. nat. Michael Bantel*** at Hochschule Karlsruhe Technik und Wirtschaft.

I declare that all observations, analysis and results are solely mine and have not been published by or in any other sources. Any references used for the work have been cited at the respective position and listed in the References.

This Master Thesis is submitted as a part of M.Sc Sensor Systems Technology at Hochschule Karlsruhe-Technik und Wirtschaft.

I declare that this thesis has been solely written by me and no other references, other than the ones cited here in the report has been used during the preparation.

Kesavadas, Priyanka

Karlsruhe, 15.08.2020

Acknowledgement

First and foremost I would like to extend my sincere gratitude to ***Prof. Dr. James Anthony Hinton*** for allowing me to conduct my work in his wonderful team at Max-Planck-Institut für Kernphysik.

I would like to thank my supervisor ***Prof. Michael Schmelling*** for constantly guiding me throughout the entire thesis work, patiently listening to my doubts and for being a constant source of inspiration , my professor and referee at Hochschule Karlsruhe, ***Prof. Dr. rer. nat. Michael Bantel*** for giving me this opportunity to pursue my thesis at such an esteemed institution and also for the constant support and also my co-referee ***Prof. Dr. techn. Herman-Jalli Ng***.

I would also like to thank my project head, ***Mr. Hendrik Borras*** for always cooperating with me, instilling great ideas and helping me and also my colleague ***Ms. Swathy Ramakrishnan*** for her generous support.

I also express my gratitude towards all the personnel at the Electronics Department who provided constant help and guidance for the progress of this work.

Last but not least, I would like to thank God Almighty, my family and friends for their moral and financial support and for giving me strength and hope for the completion of my work.

List of Abbreviations

LHCb – Large Hadron Collider beauty

SiPM – Silicon Photomultiplier

DAQ – Data Acquisition System

GPS – Global Positioning System

CosMO – Cosmic Muon Observer

UTC – Universal Time Coordinated

DESY - Deutsches Elektronen-Synchrotron

PCB – Printed Circuit Board

USB – Universal Serial Bus

JFET – Junction Field Effect Transistor

Contents

Chapter -1

Introduction

1.1 MPIK

Max Planck Institut für Kernphysik (MPIK), located in Heidelberg, Germany, is one of the 80 institutes belonging to the Max Planck Society[1]. The MPIK was established in 1958, headed by Wolfgang Gentner and focuses on two main research areas: Quantum Dynamics and Astroparticle Physics[2]. There are five departments at present specializing in different aspects of these main areas at the MPIK. This work was conducted within the department of non-thermal astrophysics, which is headed by Prof. Dr. Jim Hinton, and more specifically within the LHCb (Large Hadron Collider beauty) group of this division.

1.2 Motivation

Muons are elementary particles of Physics, about 200 times heavier than electrons and only subject to electromagnetic and weak interactions, which makes them highly penetrating and hence also useful in applications involving the study of large structures, probing of various topographies and in general also to enhance the understanding of the world around us. Thus, the detection of muons and the analysis of this data prove to be quite critical and important. Critical parameters that characterise the performance of a detector are noise, average pulse height and duration, which all contribute to the detection efficiency. Technically these characteristics are determined using various tools like e.g. ROOT Software from CERN[3], which allows one to create visualizations of the obtained data and also to understand how well the improvements help the board in an increase in the detection of muons. The development of a mobile and optimized detector will allow students and amateurs to understand the particle, its detection and various features.

Cosmic ray muons have the ability to penetrate deep into various surfaces due to their heavier mass. Given that the earth's inner atmospheric layer, the mesosphere, extends up to a distance of 90km to 100 km, only a very small fraction of muons created by the interaction of primary cosmic rays with the earth's atmosphere, of approximately 1 per cm^2 per minute reaches the ground level. Since the charge deposited by a passing muon inside a semiconductor diode is quite small, the typical signal that is obtained will also be of the order of a fraction of a millivolt along with a significant amount of noise. Due to the low incidence rate of particles, it is required to take the data for the analysis over a large amount of time. Taking data over a long time allows us to see more events as we need to see enough events to do reliable analysis. An analysis of the noise levels too can provide information about the signal to noise ratio.

1.3 Objective

The Silex version 1 board was the first version of this Cosmic ray muon detector developed around multiple PIN-Diodes, with an arrangement of 10 diodes for detection. This was followed by version 2 and 3, each having a different arrangement of 50 diodes on each board, of which the version 3 Silex boards are the latest version which are to be analysed for their performance. The main objective is to conduct a performance analysis of the Silex version 3 cosmic ray muon detector boards with the changes made to the previous version and to optimize the new version for a better and more efficient detection. The data obtained from the prototype boards can be used to understand important details of the developed Silex detectors through various methods like averaging and normalization, scatter plots, detector efficiency calculation and signal to noise calculation. The analysis can help in optimization of the boards.

Chapter - 2

Cosmic ray muon detection

2.1. Muons

Muons are elementary particles of matter classified as second generation leptons. They are heavier than electrons, which belong to the first generation leptons. Muons also decay to electrons and neutrinos. They are unstable particles with a mass of 105.66 MeV/c^2 and a spin of ½[4]. Muons are represented by the Greek letter μ and have a charge of -1 e. They have a corresponding antiparticle, the antimuon with opposite charge and equal spin. Muons, being much heavier than electrons, are less affected by Bremsstrahlung, thereby allowing them to penetrate deeper into various materials. Bremsstrahlung works such that a charged particle traveling through a material is deflected from its path by other charged particles, thereby causing deceleration due to which a decelerating radiation or Bremsstrahlung radiation is emitted[5]. But in the case of muons, their heavy mass leads to less deceleration, thereby reducing the Bremsstrahlung radiation. The main energy loss mechanism for a muon traversing matter thus is ionisation energy loss. Muons are formed mainly in processes involving high energies, such as within secondary cosmic rays where high energy collisions occur. The average lifespan of a muon is 2.2 μs[6].

2.1.1. Muon formation from cosmic rays

The main component of the primary cosmic rays are protons. When these enter the earth's atmosphere they undergo inelastic interactions with atomic nuclei in the upper atmospheric layers at a height of about 30km resulting in the formation of secondary cosmic rays. Secondary cosmic rays comprise of π mesons (pions) which decay to form muons. During the decay of pions, both a muon and muon neutrino are created, and the muons continue at

almost the speed of light and in about the direction of the cosmic ray proton[7]. This is depicted in Figure 2.1.

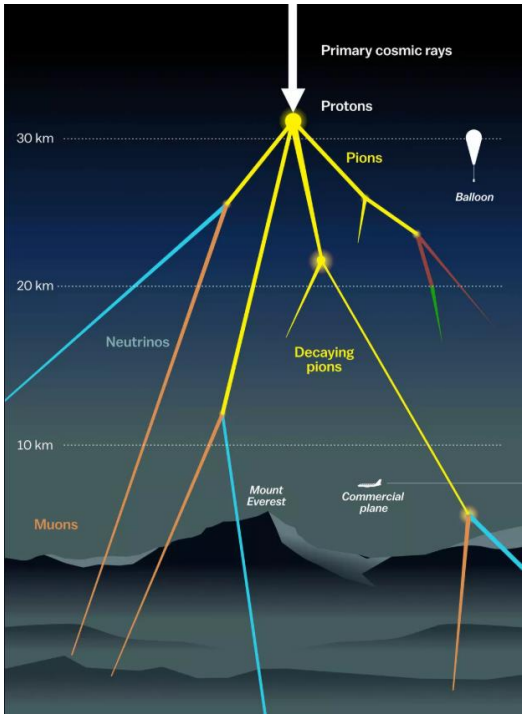

Figure 2.1

Cosmic ray muon creation[8]

Muons decay into electrons and neutrinos as shown in equation (1) through weak interactions in about 2 μs:

$$\mu^- \longrightarrow e^- + \nu_{\bar{e}} + \nu_{\mu} \qquad (1)$$

2.2. Cosmic Ray muon detectors

Various cosmic ray muon detectors have been developed for muon detection, with the main component being scintillators. Whenever a muon passes through a scintillator, it produces photons which are then detected by a photomultiplier. Photomultipliers produce electrical signals when photons are detected. Compared to traditional photomultiplier tubes, silicon photomultipliers (SiPMs) require less power and significantly lower operating

voltages, which makes the entire design compact and thus mobile. They are also cheaper than most other photomultipliers. Such a detector setup is provided by CosMO experiments available from Netzwerk Teilchenwelt. [24]

Here the amplified signal from the SiPM is sent to a data acquisition system (DAQ) which decides on which is a potential signal. The resulting data are displayed using the oscilloscope and also sent to a CosMO computer where they can be stored for further analysis. A GPS-unit used along with the DAQ allows to synchronize the received data to UTC. Figure 2.2 shows the experimental setup used in this work. The data obtained from the setup with the scintillators verifies the data obtained from our prototype boards. The analysis of the recorded data is then done at a later point in time.

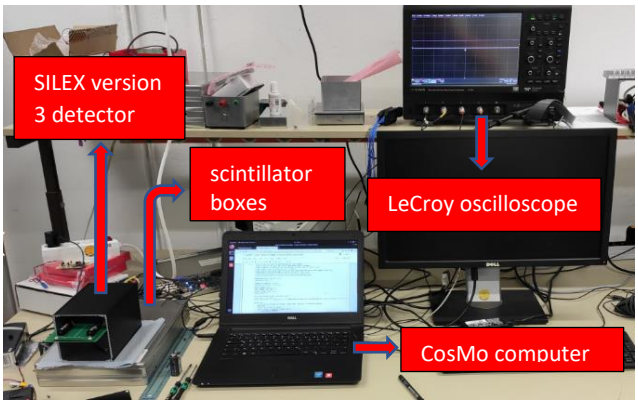

Figure 2.2

Experimental setup

2.2.1. CosMO detector

The CosMO detector is a muon detector for cosmic rays developed at the Deutsches Elektronen-Synchrotron (DESY), in order to allow students to study cosmic muons and their features. This experiment consists of scintillator boxes, a data acquisition card for triggering events and a laptop, equipped with a Python program written for Linux which helps to read and store the data for further analysis. The CosMO detectors are used at present in several research institutes and universities[9].

2.2.2. Scintillator

Certain materials, such as polyphenyl hydrocarbons and NaI (TI), produce light upon being hit by a charged particle. This is the property of scintillation, which in particle detectors, can then be used along with photomultipliers to produce electrical signals when an ionizing particle passes through the material[10]. There are various types of scintillators like plastic scintillators, inorganic crystals, glass, liquids and gases. The CosMO detector used in this thesis utilizes a plastic scintillator with an area of 200x200 mm^2.

2.2.3. DAQ card

The data acquisition (DAQ) card allows one to discriminate signal and noise automatically. When a signal pulse is found, the DAQ card produces a trigger pulse which can be displayed on the oscilloscope. It takes in signals from each channel connected to the top and bottom scintillator boxes respectively, and using a discriminator decides if the signal contains an event, which in this case is a threshold of 30mV for each channel. Additionally the card determines coincidences between the multiple input channels. The DAQ card also contains a microcontroller with which different parts of the board are setup and configured. Communication is realized, via a USB connection between the CosMO computer and the DAQ card[11]. The DAQ card when used along with a GPS unit allows one to synchronise the obtained data with the global UTC time, thus making it possible to synchronize multiple independent setups.

2.2.4. CosMO computer

A notebook computer running Ubuntu 18.04 LTS is used for the CosMO detector. This computer allows to communicate with the DAQ card using a USB cable and also has a software developed by the "*Netzwerk Teilchenwelt*" for receiving and storing the data from the DAQ card. Within this work the

laptop is also used to communicate with the LeCroy scope and custom Python software is used to read and store data from the scope.

2.2.5. Oscilloscope

If a coincidence is found in the DAQ-card, a digital pulse is sent to the oscilloscope to be displayed in real time and screenshots of the traces produced can also be captured on the oscilloscope. The Oscilloscope used in the project is a LeCroy HDO6104-MS[12] . The oscilloscope has 4 analog input channels and 16 digital channels. The analog channels have a resolution of 12 bits which can be enhanced to 15 bits with enhanced resolution (ERES). The digital pins are used to connect the DAQ card with the oscilloscope. There are also 2 ethernet interface RJ45 ports, which are used in the current work to connect the CosMO computer and the oscilloscope so that they can communicate with each other. Figure 2.3 shows the LeCroy scope used for this work.

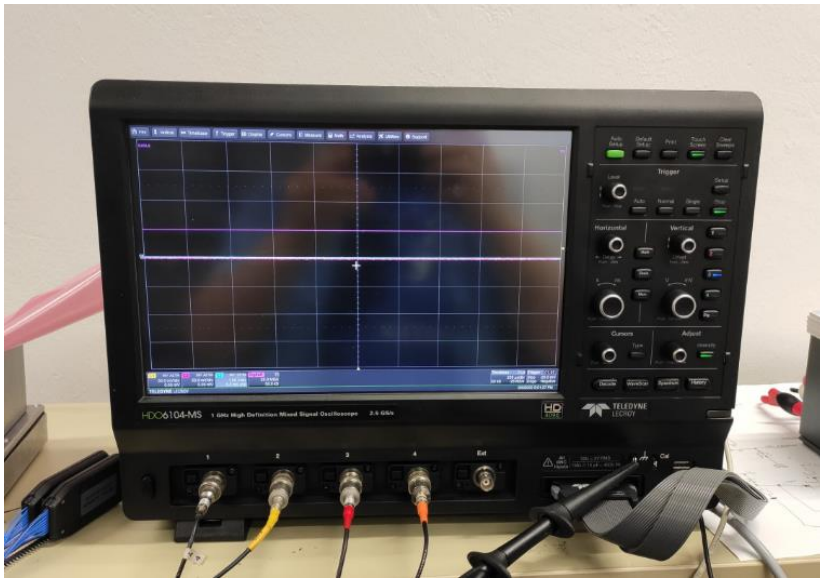

Figure 2.3
LeCroy HDO6104-MS

2.3. Detector setup

In the current setup, there are two prototype boards, the top board and the bottom board, each with 50 PIN diodes. The system is placed above the CosMO scintillators that serve as a reference. The scintillators, upon detecting a muon emit visible-light photons which are detected and converted to corresponding electrical signals by SiPMs. The DAQ card recognizes the potential signal which is then communicated to the CosMO computer. The PIN diodes on the boards perform the combined task of scintillator and SiPM by giving an electrical signal output for muon detection. Muon detection takes place due to ionization within the diodes, when an ionizing particle passes. This signal is then passed to the circuitry provided on the boards consisting of amplifiers and filters which help in reducing the noise and giving a good output signal that can be viewed on the oscilloscope and analysed further. The entire setup of the boards are placed inside a light-tight box. Thus the earlier bulky setup of scintillators, SiPMs and DAQ board are replaced by a comparatively smaller box consisting of two thin PCBs. This entire setup can be powered using a USB supply or batteries which makes it easy to handle. The oscilloscope can be interfaced with the CosMO computer to communicate and exchange data.

Chapter -3

SILEX Detector

3.1. Detector board design

The cosmic ray muon detector consists of two boards each equipped with 50 PIN-diodes that produce electrical signals when a particle of cosmic radiation is detected. These diodes are connected to a JFET in bootstrap, which in turn is connected to a two stage amplifier. The signal then is given to a high pass filter to filter out the low frequency noise, followed by an impedance decoupling to match the output signal to the ADC of a micro-controller as foreseen for the final system. The boards are provided with a 4.5V power supply with the help of an on-board linear regulator. In order to obtain coincidence measurements, both boards are setup overlapping each other and are connected using on board spring connectors. These boards are then placed in a grounded isolation box equipped with connectors connecting the boards to the oscilloscope. The box is placed on top of two scintillator boxes in order to verify the output obtained. The entire setup is shown in Figure 3.1.

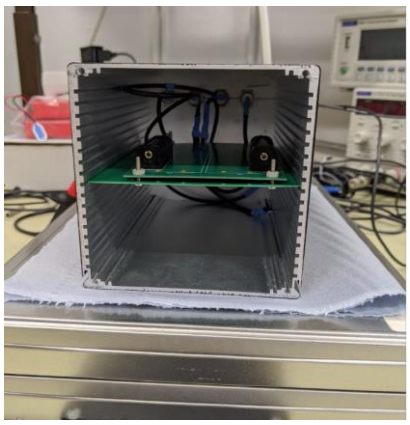

Figure 3.1
Silex version 3 and CosMO detector setup

3.1.1. PIN Diodes

PIN Diodes are pn-junction diodes with an intrinsic 'I' region in between, made of Silicon semiconductor material which has high resistance. PIN diodes have a very small junction capacitance and are current controlled devices[13]. Most of the cosmic radiation particles ionize silicon within a very short time and this ionizing radiation will deposit charge within the PIN diodes. When used in forward bias condition, they work as a variable resistor in microwave and RF frequencies, but here we exploit the reverse bias feature of PIN diodes. When in reverse bias condition, the depletion region increases and the diode is now similar to a capacitor. The intrinsic layer consists of silicon that is ionized by passing charged particles. As a result, passing muons will ionize the silicon and cause a reverse current which can then be observed by connecting these diodes to external circuitry. The PIN diodes used for the project are BPW34 SMD[14] diodes with an active area of 8 mm^2 (2.83mm x 2.83 mm).

3.1.2. Top board

The top board consists of a rectangular row-wise arrangement of 50 PIN diodes with approximately 1.5 cm^2 (50 x 2.83 mm^2) active area of the board. The board is a PCB with a thickness of 0.8 mm with the bottom side being filled by a grounding layer throughout the board, except at a small underneath the amplifier stage. The reverse side of the top board as shown in Figure 3.3 has a provision of attaching batteries which provide bias voltage to both boards.

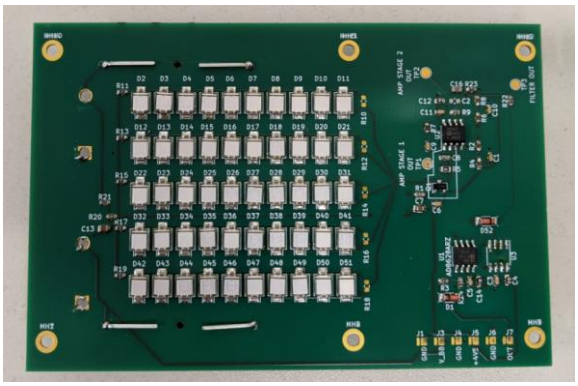

Figure 3.2
Silex version 3 top board front view

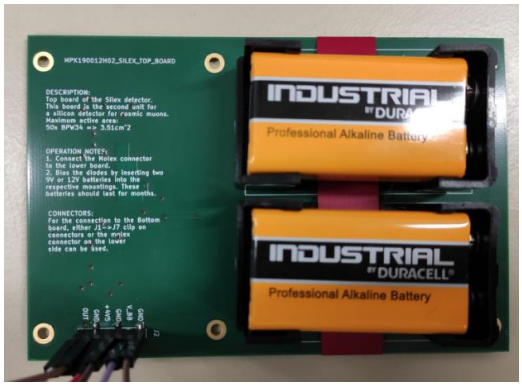

Figure 3.3
Silex version 3 top board back view with 9V batteries

In the Figure 3.3, 9V batteries are used to provide the bias voltage. These were later replaced by 12V batteries, which are more compact than the 9V ones. A provision to include both types of batteries on the board as per convenience is provided. Depending on the requirements, the appropriate battery can be used along with its battery holder. The reverse side of the top board along with 12V batteries is shown in Figure 3.4.

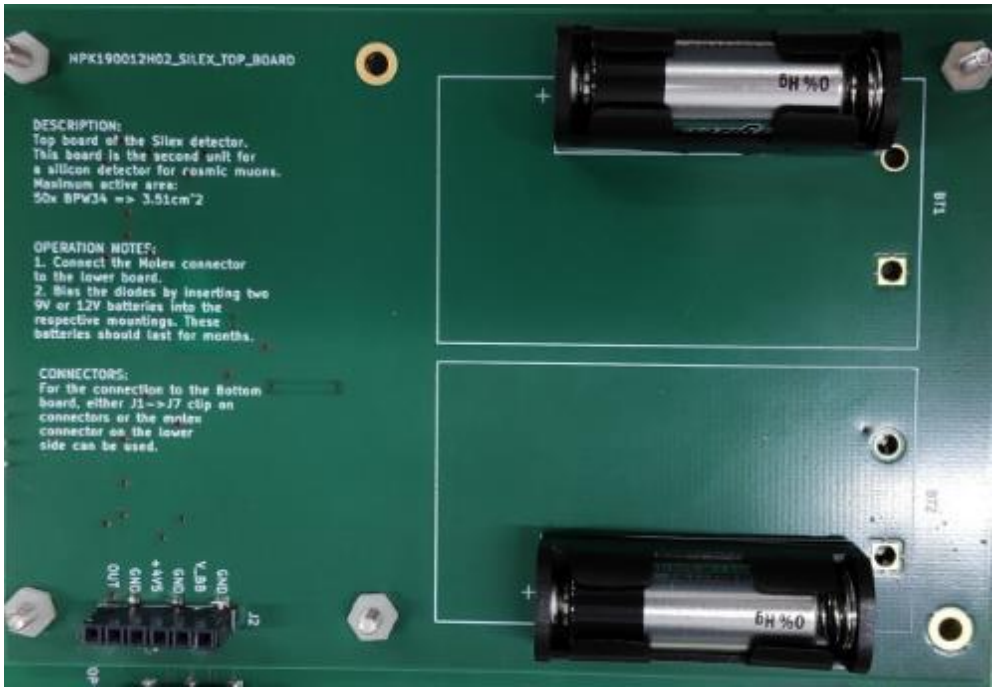

Figure 3.4
Silex version 3 top board back view with 12V batteries

3.1.2.1. Amplifier stage

The amplifier stage has two AD8629 op-amps that provide a two stage amplification as shown in Figure 3.5, with the signal to these op-amps coming from a BF862 JFET connected in bootstrap mode[15] so as to reduce the noise and capacitance as seen by the following op-amps. The electrical signal from the PIN diodes is sent to this amplification stage, thereby helping to amplify and produce a good signal from the detected weak one. Figure 3.5 shows the amplifier stage circuit diagram.

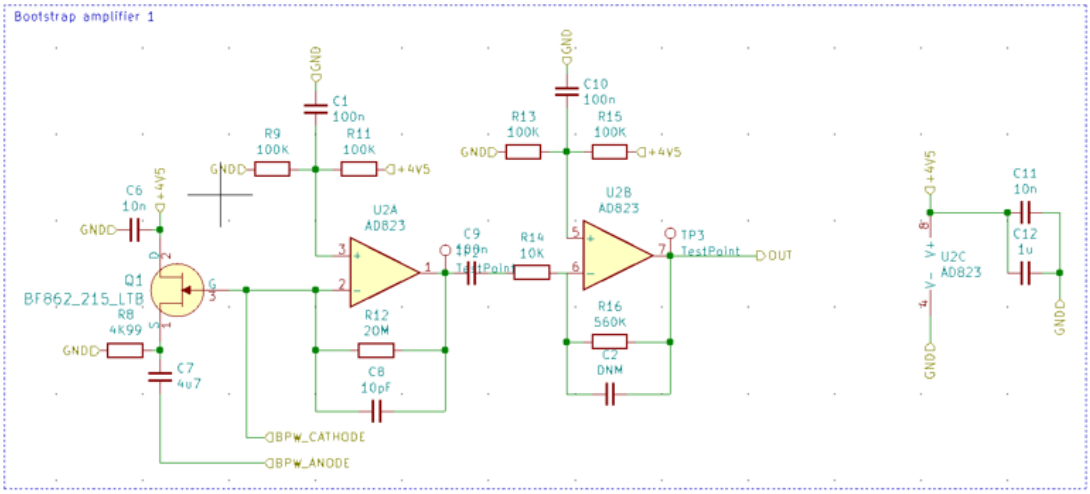

Figure 3.5
Amplifier stage

3.1.2.2. Filter and decoupler stage

Though the obtained signal has been amplified, it still contains noise which contaminates the required output signal, and since low frequency noise was most dominant, we use a high pass filter followed by an impedance decoupler that helps reduce the physical inductance and widens the impedance bandwidth. Figure 3.6 shows the circuit diagram for the filter decoupler stage. The outputs of the boards are intended to be given to a microcontroller which has an ADC unit and in order to protect this a protective Zener diode is used here (D52).

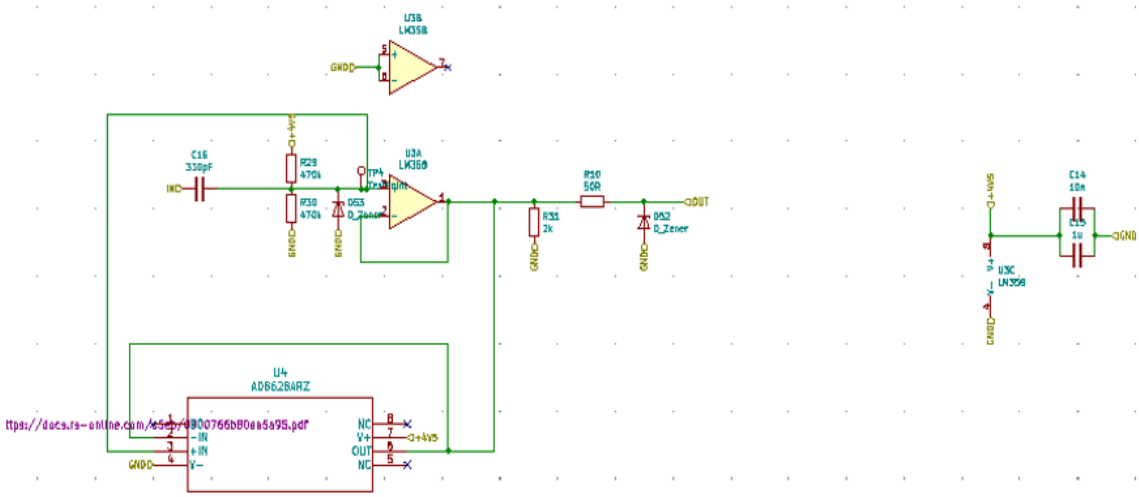

Figure 3.6
Filter decoupler stage

3.1.3. Bottom board

The bottom board consists of a similar rectangular row-wise arrangement of 50 PIN diodes as on the top board as shown in Figure 3.7. This board is also a PCB with a thickness of 0.8 mm with the bottom side being filled by a grounding layer throughout the board, except at a small area underneath the amplifier stage. Unlike the top board, the bottom board also incorporates a linear regulator circuit on the reverse side as seen in Figure 3.8. The bottom board has no batteries for biasing since all bias voltage is supplied by the top board to the bottom board.

Figure 3.7
Silex version 3 bottom board front view

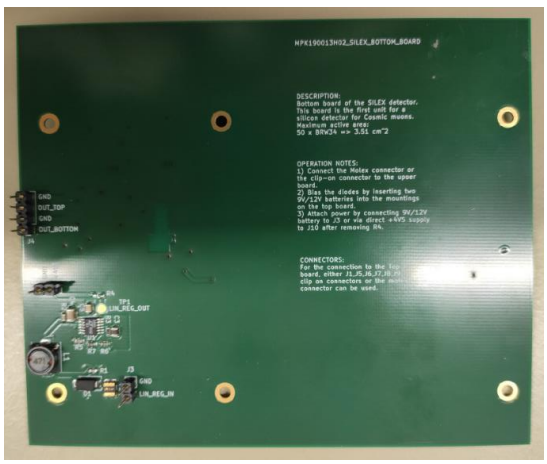

Figure 3.8
Silex version 3 bottom board back view

3.1.3.1. Linear regulator

The LT3045 IC is used for the linear regulator circuit, which helps to provide a steady 4.5V supply to the boards and is depicted in Figure 3.8. The input can be given either from the batteries or a USB supply. The circuit as such supports voltages up to 20V thereby allowing one to explore other power options in the future. Currently 9V batteries or a 5V USB connection are used to provide the supply. The linear regulator output is used as the supply for both boards and the utilization of a polyfuse and a transient voltage suppression diode in the circuit helps to prevent any over current and any over voltage from entering the boards, which may otherwise damage them.

3.1.4. Connectors

The Silex version 2 boards used wires to connect both the boards, which can be untidy. Hence in the version 3 boards PCB spring contacts were utilized, which improved the visual design and stability, simplified the board setup and reduced the sensitivity of boards to pickup noise and noise from vibrations. Both boards are placed on top of each other with the diode layers of both boards facing each other. The boards are then fixed in place using the 6 mounting holes on the outer area of each board shown in Figure 3.9.

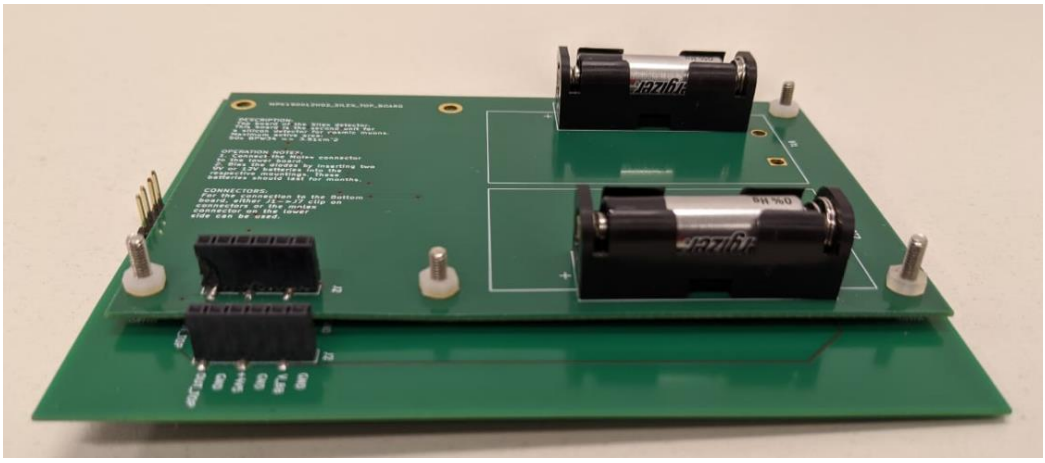

Figure 3.9

Board setup for coincidence measurement

Chapter -4

Theory on Data Analysis

4.1. ROOT Software

ROOT [https://root.cern] is a data processing software developed at CERN. It is a software package and program library which is written in the C++ programming language and helps in accessing, storing and analysing data. The software package also contains a C++ interpreter (CINT), which allows users to interactively use different parts of the ROOT library. Additionally bindings to other programming languages are readily available, like pyROOT [https://ph-root-2.cern.ch/manual/python/]. It is an Object Oriented program and was developed with the intention of allowing one to easily work with various data, perform simulations and analyse them. The test data obtained for the project is read and traces are displayed using ROOT. The software also helps to read and run an analysis program written in C++, which was used to work on the test data obtained in order to understand various parameters of the traces obtained.

4.2. Analysis techniques

Even though the project uses an oscilloscope to display the acquired signals in real time, further understanding of the working and efficiency of the detector and of the signals obtained can only be done through a detailed analysis. For this purpose, test data for various design modifications is recorded over a period of 3-12 hours and saved on the CosMO computer. This serves the process of optimization. Various parameters of the data obtained can be explored using a number of mathematical techniques like averaging, normalization and correlation analysis. Critical parameters like the height of the waveform obtained, noise in the traces, maxima plots, efficiency

and signal to noise ratio can be analysed. The comparison of all these parameters for various modifications will result in an optimised design that improves the boards detection capabilities. The test data for the project has 250 samples for each trace/waveform obtained. When read initially from the oscilloscope, there are 25000 samples per trace with the sampling rate of the scope set to 25 Msamples/s. These traces were later averaged in bins of 100 samples such that new traces with 250 samples were obtained, where each sample is actually an average of a 100 samples from the original trace[23]. This allows to reduce the data size and simplify analysis. The total number of traces/events 'N' can be input in the program for the analysis. The performance of the detector can be analysed using two methods:

i. *Average-based analysis*

   Here all the traces are averaged such that noise cancels and mostly the signal remains. To obtain a prototypical signal trace the averaged trace is then normalized. Convolving the prototypical trace with each trace of a measurement attributes a score to each trace. This score determines how close a measured trace is to the prototypical signal. Plotting for each event the scores from both boards as a scatter plot tells us how well the signal and noise separate. This can be used to find the efficiency of the individual boards.

ii. *Event-based analysis*

   Here the RMS noise is calculated from the downward fluctuations of each trace. The signal is determined from the upwards fluctuations with a few additional operations to select coincidence events. This allows one to obtain the signal to noise ratio and also the efficiency of the setup. The details regarding the analysis are discussed in the following section 4.2.3.

4.2.1. Averaging and Normalization

Averaging helps in understanding the overall features of a large number of similar data and this, when followed by suitable normalization, brings all data to a same scale where they outline the general shape or pattern of the traces.

Suppose there are N number of traces where each trace is represented by $\vec{X}_i$ where i = 1,2,....N traces and $\vec{X}$= {x_1, x_2.....x_{250}}, as each individual trace x_j has 250 samples.

The averaged waveform of these N traces are,

$$\vec{a}_j = \frac{\sum_{i=1}^{N} \vec{X}_i}{N} \quad (2)$$

where $\vec{a}$ is the averaged vector of all the N traces such that $\vec{a}$ ={a_1,a_2,....a_{250}}

Here, each individual average sample is in itself an average of the corresponding trace samples. For e.g.,

$$a_1 = \frac{\sum_{i=1}^{N} X_{i1}}{N} \quad (3)$$

Now, the normalization is done on this averaged trace vector through linear transformation on all individual elements to obtain the vector

$\vec{n}$ ={n_1,n_2,....n_{250}}, with elements

$$n_j = \frac{a_j - \mu}{\sigma} \quad (4)$$

where μ, which is the mean value of all measured datapoints, can be found by

$$\mu = \frac{\sum_{j=1}^{250} a_j}{250} \quad (5)$$

and the standard deviation σ can be found by,

$$\sigma = \sqrt{\frac{(a_j - \mu)^2}{250}} \quad (6)$$

The normalization allows to bring data in different ranges onto same range for better comparison.

4.2.2. Scatter Plots

Scatter plots are one of the most widely used visual data analysis tools. A scatter plot uses cartesian coordinates to plot two related variables, thus allowing to understand the correlation between the two data sets[16] . Correlation is basically the dependence of a parameter of interest on another parameter.

There can be various types of correlations like,

i. Correlation, which results in a linear rising with positive slope of both variables.
ii. Anti-correlation, which results in a linear falling with negative slope of both variables
iii. No correlation, which is when the points are randomly plot with no dependence on each other.

Since in the project there are two prototype boards which are placed on top of each other, an important analysis to detect coincidence measurements is the study of correlation between the boards by means of ``scores" (defined below), which show how similar a given trace is to a prototypical trace.

Let us consider the averaged and normalized vector $\vec{n}$ from equation (4) in the section 4.2.1. Then the 'score' is calculated by the scalar product of the vectors X and n,

$$F = \vec{X} \cdot \vec{n} = \sum_{i=1}^{250} X_i \cdot n_i \qquad (7)$$

Now, the value of F will be 0 if the $\vec{X}$ is constant, and will have a positive value if $\vec{X}$ has a signal component. This means that F (score) shows how similar a given trace is to the average signal. Thus, from a scatter plot as shown in Figure one can observe F_{top} on the y-axis which shows the top board score and F_{bot} on the x-axis which shows the bottom board score.

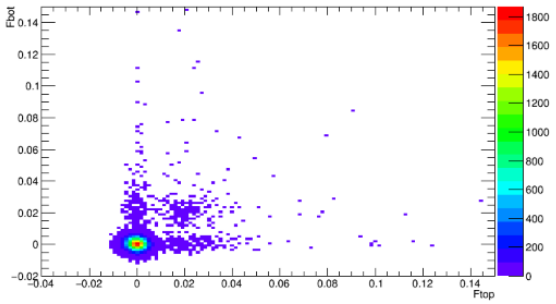

Figure 4.1
Scatter plot

From this plot, one can observe any coincidence which happens between the boards, how well the signal is distinguishable from the noise and how often there is a signal only on one of the boards.

4.2.3. Efficiency

The efficiency of the detector can be defined as the ratio of muons that pass a diode, giving a visible signal to the total number of muons that pass the diode.

4.2.3.1. Monte Carlo simulation

A Monte Carlo simulation is used to simulate muon count rates. The coincidence counts that are obtained from here can be used along with the actual coincidences that one gets from an analysis in order to obtain the efficiency. Let us first consider the various possibilities of passing muons as shown in Figure 4.2. They can pass:

i. Only through the scintillators
ii. Through any one diode
iii. Through both the diodes
iv. Through any one diode and the scintillators
v. Through the scintillators and both diodes

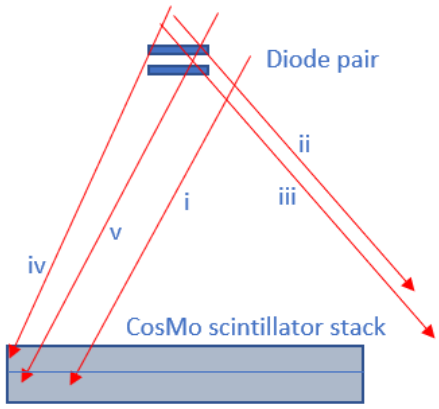

Figure 4.2
Muon hit possibilities
[The figure is not to scale]

For carrying out the simulation, the geometry of the setup is required.
We utilize two scintillator boxes of height 28 mm stacked on top of each other each with an effective area of 200 x 200 mm^2 and the pin-diodes are 50 x 2.83 x 2.83 mm^2. The active area of the diode was found to be square with a 2.83 mm edge length by calculating the inner region area of the silicon within the diode, which had dimensions of 2.815 mm to 2.846 mm. Thus the edge of the active area was found to be (2.815+2.846)/2 = 2.8305 mm[22] .
A cross-section of the diode is as shown below in Figure 4.3.

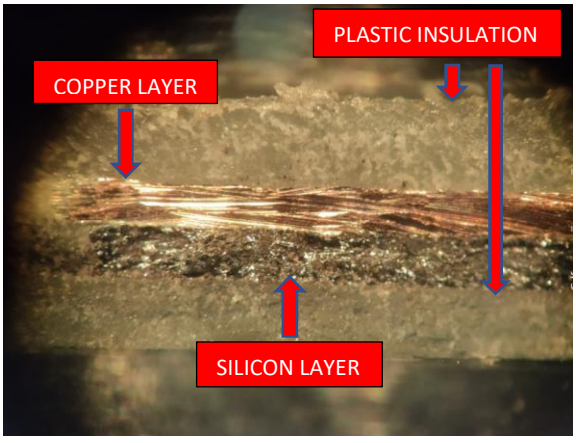

Figure 4.3
Cross section of BPW34 SMD diode[22]

The distance between both the scintillator boxes is 28 mm and between both diodes is 1.95 mm, whereas the distance between the diodes and the scintillators is 88 mm[24].

The fraction of PIN-diode events that will have a signal is <0.01. This upper limit can be obtained by the ratio of the area of the diodes and the scintillator, which are (50 x 2.83 x 2.83 mm^2)/(200 x 200 mm^2) = 0.01.

In order to simulate the angular distribution of muon flux a parametrisation of the form,

$$\frac{dI}{d\Omega} = I_0 \cos^2\theta \tag{8}$$

is assumed with,

$$d\Omega = \sin\theta \, d\theta \, d\phi \tag{9}$$

I_0 is the muon flux (muons/ mm^2 s)

dΩ is the solid angle element

θ is the zenith angle with respect to the vertical direction

Φ is the azimuth angle around the vertical direction

Since the flux through a horizontal area will have an additional factor of cos θ, the resulting angular distribution of muons through the horizontal direction will be,

$$\frac{dI}{d\theta} \propto \sin\theta \cos^3\theta \tag{10}$$

$$\frac{dI}{d\phi} \propto 1 \tag{11}$$

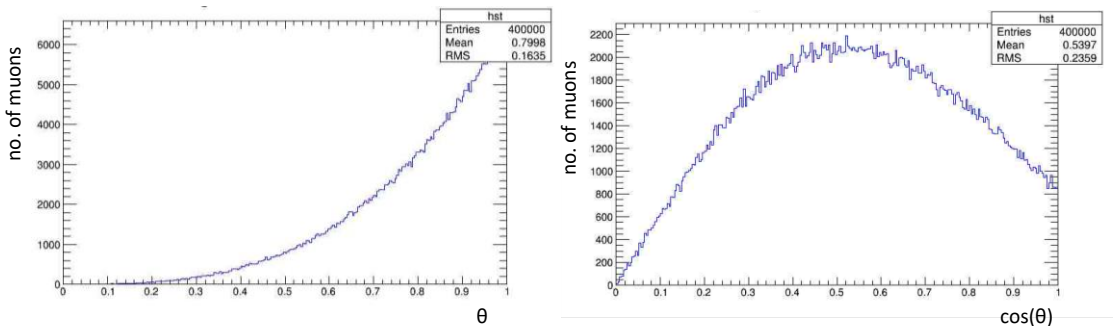

(a) (b)

Figure 4.4 angular distribution of muons : (a) θ distribution (b) cos(θ) distribution

Since the data requires a trigger on the scintillators, we assume that the scintillator sees all the muons that pass through, and a simulation is performed to find the geometric muon acceptance probabilities for the various conditions shown in Figure 4.2. First, a muon hit (x_0, y_0) is generated on the scintillator uniformly over the area of the scintillator. Figure 4.5 (a) and (b) shows the coincidence positions over the scintillator 1 and 2 respectively.

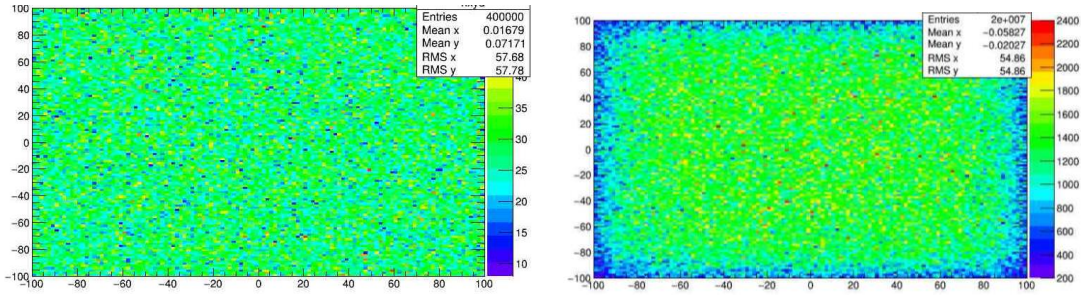

(a) (b)

Figure 4.5 muon hit on (a) scintillator 1 (b) scintillator 2

The direction angles θ and Φ is generated using the equations (10) and (11). The direction vector,

$$\vec{n} = (n_x, n_y, n_z) \tag{12}$$

is given by,

$$n_x = \sin\theta \cos\phi \tag{13}$$

$$n_y = \sin\theta \sin\phi \tag{14}$$

$$n_z = cos\,\theta \tag{15}$$

This allows us to extrapolate the distance dz_1 from the top diode to the scintillator (x_1, y_1).

$$x_1 = x_0 - d_{z1}\frac{n_x}{n_z} \tag{16}$$

$$y_1 = y_0 - d_{z1}\frac{n_y}{n_z} \tag{17}$$

Similarly, the distance dz_2 from the bottom diode to the scintillator (x_2, y_2) can also be extrapolated using the equations (16) and (17). Figure 4.6 (a) and (b)

shows the coincidence positions on the top and bottom board diodes respectively.

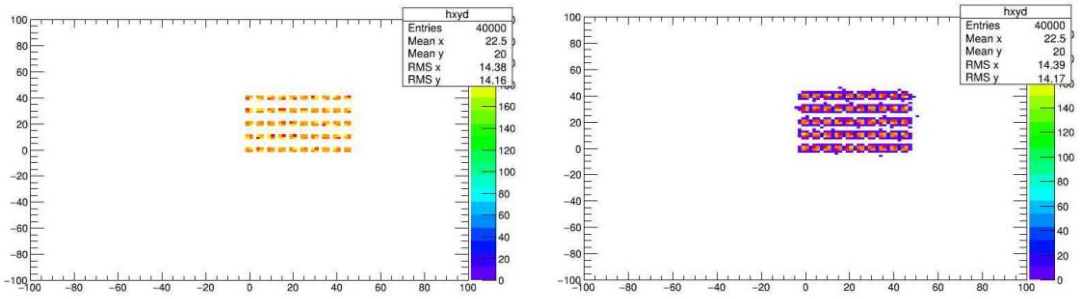

(a) (b)

Figure 4.6 coincidence positions on (a) top board (b) bottom board

The position from the bottom scintillator to the top scintillator can be calculated by equations (18) and (19).

$$x_{1s} = x_0 - d_{zs}\frac{n_x}{n_z} \tag{18}$$

$$y_{1s} = y_0 - d_{zs}\frac{n_y}{n_z} \tag{19}$$

Coincidences are determined by looking at the distance between a muon hit (on the top or bottom board), from the center of each diode. If the distance between the impact point and on the diode and the center is in both dimensions less than the half width of the diode in question, then there is a muon hit on that diode. If both diodes have a hit, then there is a coincidence. In order to find the efficiency of the boards, the following coincidence conditions considered are:

acc_{34} – coincidences between the scintillators

acc_{134} – coincidences between the bottom board and scintillators

acc_{234}– coincidences between the top board and scintillators

acc_{1234} – coincidences between both the boards and scintillators

The acceptance probabilities can also be calculated from these parameters. It is basically the ratio of each of these parameters with acc_{34}.

4.2.3.2. Average based analysis

The average based analysis utilizes the scatter plots. From the obtained scatter plots, the event scores for each board as well as their coincidence can be obtained by separating the sections using horizontal and vertical cuts as shown in Figure 4.7 (a) and (b).

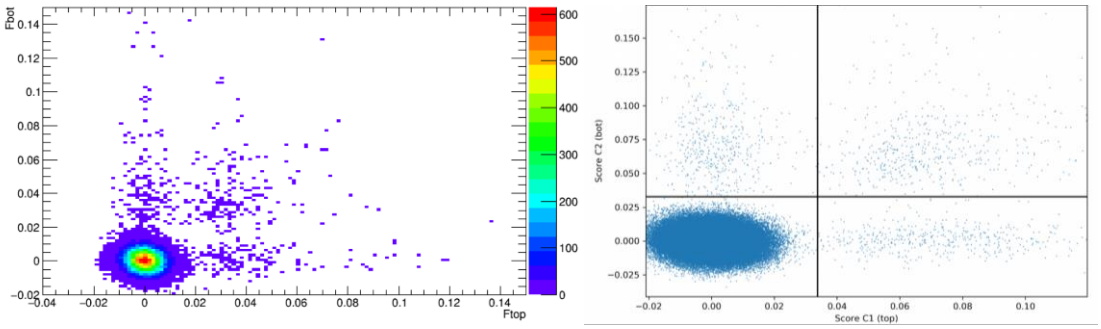

(a) (b)

Figure 4.7 average based analysis: (a) scatter plot (b) Cuts for efficiency calculation[22]

In Figure 4.7 (a), a heat map of a scatter plot is shown with the x axis having the top board score and y axis having the bottom board score. We need to count the scores for each board individually as well as their coincidence. We also need to separate out the noise region. This can be achieved with the help of two cuts, horizontal and vertical, as shown in Figure 4.7 (b). All events that occur to the right side of the vertical cut are coincidences of the top board and scintillator and all events to the top of the horizontal cut are coincidences of the bottom board and scintillator. The top right section indicates the coincidence between both boards and the scintillator while to bottom left section indicates the noise. The counts obtained from each region can be used to calculate efficiency of the individual boards with the help of the parameters obtained during Monte Carlo simulation as shown below. Here, N is the total number of events

$$\varepsilon_1 = \frac{bts}{botsc*\left(\frac{acc_{1234}}{acc_{134}}\right)} \qquad \varepsilon_2 = \frac{bts}{topsc*\left(\frac{acc_{1234}}{acc_{234}}\right)} \qquad \bar{\varepsilon} = \sqrt{\frac{bts}{N*\left(\frac{acc_{1234}}{acc_{34}}\right)}} \qquad (20)$$

where,

bts = coincidences between both boards and scintillators

botsc = coincidences between the bottom board and scintillators

topsc = coincidences between the top board and scintillators

4.2.3.3. Event based analysis

In order to do an event based analysis, first the average voltage level (baseline) needs to be determined. As an example, a trace for 20M and 10pF with a USB supply can be considered as the event x now. So there is an event x with the number of samples $i = 1,2 \dots 250$. The average $\langle x \rangle$ is

$$\langle x \rangle = \frac{1}{250} \sum_{i=1}^{250} x_i \tag{21}$$

Now the trace samples are subtracted from the average in order to centre the trace around zero. In case a signal is present, this average is slightly larger than the true baseline value. However, the bias is small and does not significantly affect the further analysis. Given the baseline level, the new trace

$$y_i = x_i - \langle x \rangle \tag{22}$$

will produce an output similar to Figure 4.8(a). The blue traces are the bottom board ones and the red traces the top board. The signal is not present in the negative portion. It is present only in the positive fluctuation along with noise whereas the negative fluctuations contain only noise. Thus, from the negative fluctuations in the Figure 4.8(a), the RMS-noise level can be determined by

$$\sigma = \sqrt{\frac{1}{N(y_i<0)} \sum_{y_i<0} y_i^2} \tag{23}$$

Figure 4.8(b) shows the noise per sample. Then from the positive fluctuations, the signal is required to be found. For this, clusters are to be formed by the summation of positive voltages over adjacent samples which results in Figure 4.8(c) and then retaining those clusters which have a total signal value > 9

times the noise. This reduces the number of clusters as shown in Figure 4.8(d). Now the required parameters can be found:

The total signal,

$$S = \sum_{i \epsilon hit} y_i \tag{24}$$

Position (centre of gravity),

$$X = \frac{1}{S} \sum_{i \epsilon hit} y_i \cdot i \tag{25}$$

RMS width,

$$w = \sqrt{\left(\frac{1}{S} \sum_{i \epsilon hit} y_i \cdot i^2\right) - X^2} \tag{26}$$

total noise,

$$N = \sqrt{\sum_{i \epsilon hit} \sigma^2} = \sigma \sqrt{m} \tag{27}$$

where m is the number of samples, and finally the signal to noise S/N is also calculated.

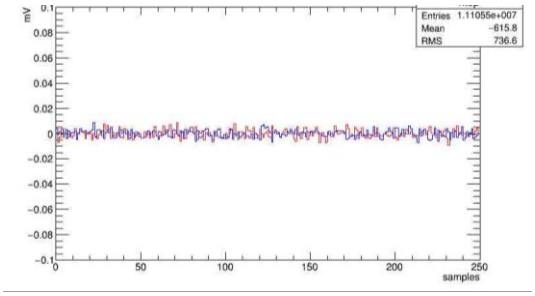

(a)

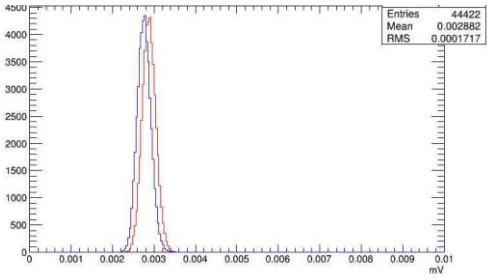

(b)

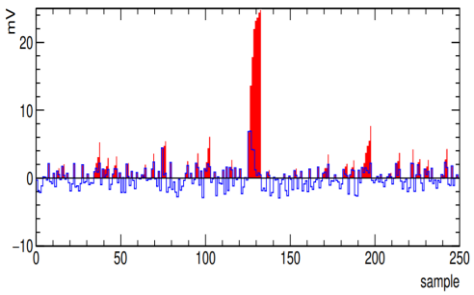

(c)

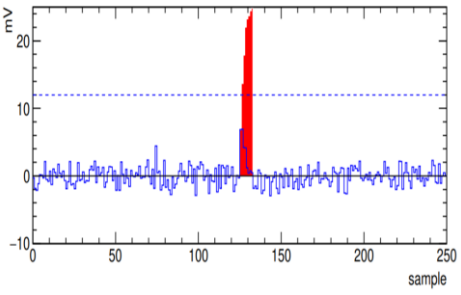

(d)

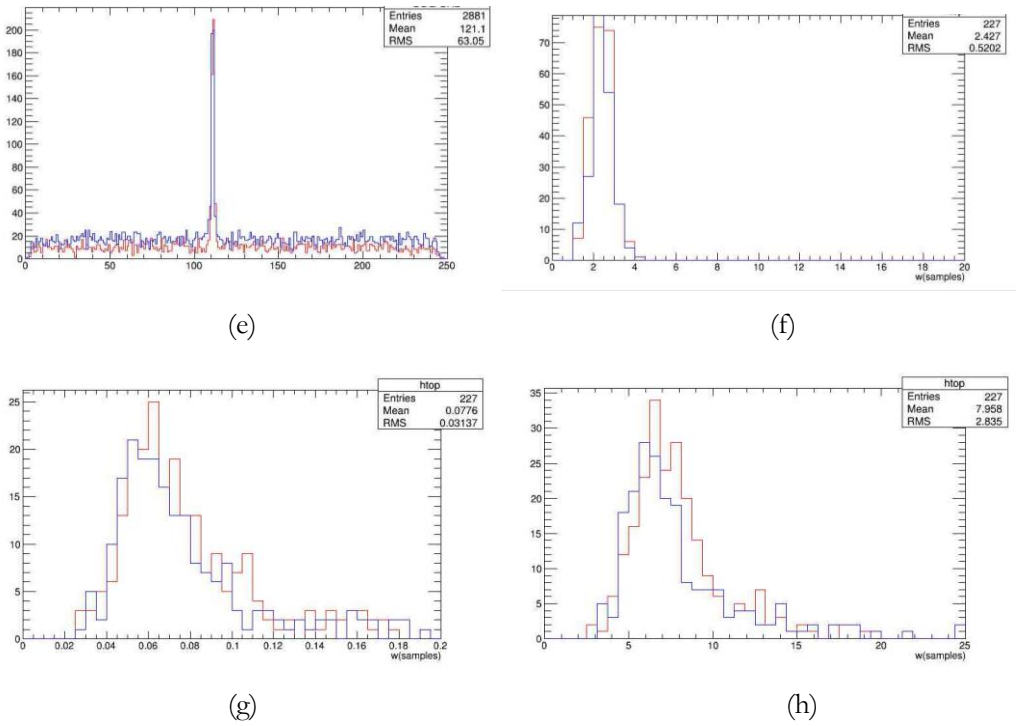

Figure 4.8 event based analysis : (a)centred and averaged traces (b)noise per sample (c)clusters of positive fluctuations (d)clusters above noise threshold (e)centre of gravity[23] (f) RMS width[23] (g)total signal (h)signal to noise ratio. [All the figures depict 250 samples = 1 ms]

Figures 4.8(e), (f), (g) and (h) show the centre of gravity, RMS width, the total signal and the signal to noise ratio respectively. The values of these parameters can be obtained for all designs and can be compared. Once the centre of gravity is found, the approximate width of the time window for a coincidence between the two boards can be determined. If signals from both boards occur within this width, then this is considered a real coincidence which occurred due to muon detection. If a coincidence occurs anywhere close to this width, but still outside the specified width, for example if the signals occur within twice the specified width, then this is taken as random coincidence due to the background noise. Now let's consider,

C_1 – coincidences between the bottom board and CosMO detector

C_2 – coincidences between the top board and the CosMO detector

C_{12} – coincidences between both the boards and the CosMO detector

From the centre of gravity plot as shown in Figure 4.8(e), one can observe a peak which represents true coincidences between the boards and scintillators whereas the other regions which seem to be almost flat contain random coincidences due to background noise. But this background noise is also present in the true coincidence region. So in order to obtain the number of true coincidences C_{12}, the count obtained from the background noise needs to be subtracted from the count obtained from the peak region. For the question of how much to subtract, a signal window is considered about the peak region and also about its sidebands which contain the background noise. The constraint used here is that the width of the sideband window equals the width of the signal window. Hence the effective C_{12} is obtained.

In order to find the coincidence count C_1, the deviation of all the signal peaks from the maximum point of the centre of gravity is determined for the bottom board, and if this deviation is less than 10 samples, it is counted as a bottom board–CosMO coincidence while the rest is considered to be noise. The fraction of the total background noise $S_n \cdot \left(\frac{N_S}{N_n}\right)$ is considered where, S_n is the total background noise obtained, N_S is the number of actual signal and N_n is the number of background noise signals.

This fraction is then subtracted from the total signal coincidences. This then gives C_1. C_2 is also found in the same manner as C_1. These parameters are then used as primary components for the rest of the analysis.

Additionally we find the geometrical parameters g_{13}, g_{23} and g_{123} where,

g_{13} is the geometrical acceptance of the bottom board diodes with the scintillator

g_{23} is the geometrical acceptance of the top board diodes with the scintillator and

g_{123} is the geometrical acceptance of the top and bottom board diodes with the scintillator.

These geometrical acceptances are obtained from the Monte Carlo simulation as mentioned in section 4.2.3.1. In principle, g_{13} and g_{23} can be separately obtained, but here they are considered equal since the difference in distance between the diodes is small, such that the difference in acceptance of the muons should also be small. One finds

$$g_{13} = g_{23} = \frac{1}{2}\left(\frac{acc_{134}}{acc_{34}} + \frac{acc_{234}}{acc_{34}}\right) \tag{28}$$

and,

$$g_{123} = \frac{acc_{1234}}{acc_{34}} \tag{29}$$

Using these counts and geometric parameters one can find the efficiency of both the boards by,

$$\varepsilon_1 = \frac{C_1}{Ng_{13}} \qquad \varepsilon_2 = \frac{C_2}{Ng_{23}} \qquad \bar{\varepsilon} = \sqrt{\frac{C_{12}}{Ng_{123}}} \tag{30}$$

where $\varepsilon_1, \varepsilon_2$ are the efficiencies for bottom and top board respectively and $\bar{\varepsilon}$ efficiency of both boards combined.

Chapter -5

Work flow

The work flow of the thesis can be divided into two major parts:

i. The optimization and analysis of the Silex version 3 boards performance using methods of averaging and normalization, efficiency analysis and event based analysis. Various issues were encountered during the testing of the version 3 boards including signal degradation, loose connectors and few others which were solved using a jitter analysis and noise plots.
ii. A basic analysis of traces obtained from the version 2 board for the same parameters which then help in the comparison of both boards.

The first part includes the various analysis techniques mentioned earlier, with the focus on the efficiency of the boards obtained. The Silex version 3 boards were tested with various combinations of resistors and capacitors in the feedback loop in the first amplifier stage which resulted in a variety of results. Certain issues like loose connectors resulted in faulty readings, which lead to the utilization of a jitter and noise analysis to rectify the problem. Additionally an analysis was also done on replacing the bulky 9V battery supply used for the bias voltage supply to both boards, with smaller 12V ones. The USB voltage supply was also investigated for its noise performance. Readings were taken while triggering on the CosMO detector.

The second part includes an analysis of the same parameters of traces obtained from the Silex version 2 boards which can tell us about the improvements achieved so far with the new design for the detector.

Chapter -6

Optimization and Results

Optimization is the process of finding a design which provides the best approximation to a desired outcome[19]. Various methods and processes were used to optimize a given design by analysing basic parameters of a waveform like pulse height, noise, time delay and jitter. The test data collected from the prototype detector boards were zipped, reduced by averaging a 100 samples into 1 out of the original 25000 samples and saved to disk in a binary format with 250 samples per trace for easier analysis due to size reduction. The ROOT software package, developed at CERN, was used as a platform to perform the analysis. The program which was developed during this thesis was written with Notepad++ in the C++ language. A link to the source code of the program used is attached in the Appendix. The test data obtained for 1MΩ and 10MΩ were done using 9V batteries as bias voltage supply, whereas the test data with 20MΩ, 47MΩ and 100MΩ used the 12V compact batteries as shown previously in Figure 3.4, as bias voltage supply. There was no significant difference in the signal obtained, but the hardware for the detector became much less bulky and easier to handle.

6.1. Traces

A single waveform or trace consists of 250 samples which is actually the compact version of the initial 25000 samples as mentioned earlier and the total number of events or waveforms per data set can be determined within the program. All the figures henceforth in this chapter depict 250 samples corresponding to 1 ms.

There is a resistor-capacitor pair in the feedback loop of the op-amp AD823 in the first amplifier stage, which makes the amplifier charge sensitive and shapes the resulting output. The output of the first stage is then amplified in

the second stage and is then sent to the filter-decoupler stage later on. Hence, proper amplification can ensure better data at the final output. 1MΩ and 10pF were the initial values for the resistor-capacitor pair in the first feedback loop with the new board design, but various combinations were tested and analysed to find the optimum pair. Resistors 1MΩ, 10MΩ ,20MΩ ,47MΩ and 100MΩ were tested each with capacitor 6.8pF, 10pF and 15pF. The readings with 10pF yielded a better result for all resistor values, except for 47MΩ giving a better result with 15pF. The x-axis in the figures shows the sample number while the y-axis shows the voltage value. The blue traces represent the bottom board signal and red trace the top boards ones. The Figure 6.1(a) has only noise and no signal. Figure 6.1(b) shows a trace with an actual signal.

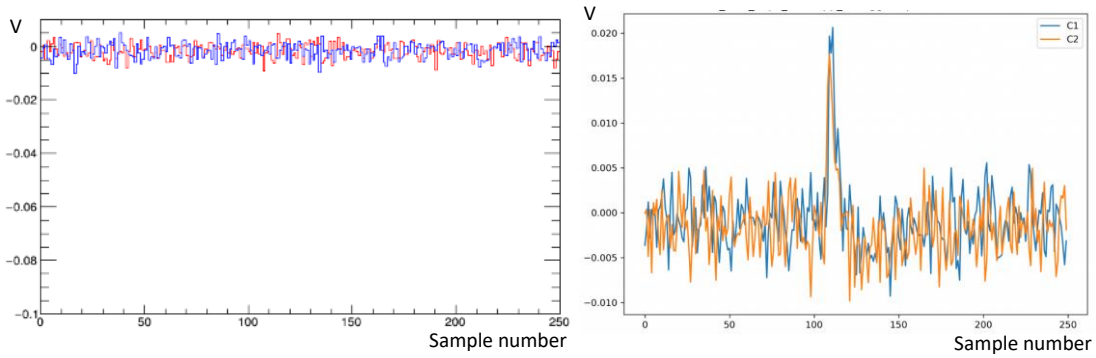

(a) (b)

Figure 6.1 traces with (a) no signal (b) signal[23]

In order to reduce cross-talk between the boards, a grounded foil was decided to be placed in between, but even though the cross-talk between the boards was reduced, the traces were found to be noisy as shown in Figure 6.2. The blue traces which represent the bottom board signals seemed to have more noise. Hence this option was rejected. Moreover the remaining cross-talk had no significant impact on detector performance. Another option of using different capacitors, i.e. 15pF on bottom board and 6.8pF on the top boards, with 1MΩ resistor used for both, in order to reduce any cross-talk between the boards resulted in a better trace shown in Figure 6.3 than the previous one, but in any case worse than the ones for all other measurements.

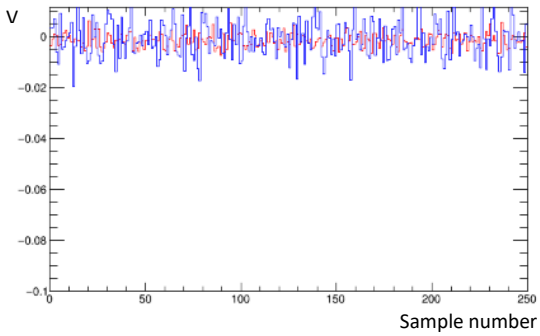

Figure 6.2

Traces for 1M Ω and 10pF
with foil between the boards

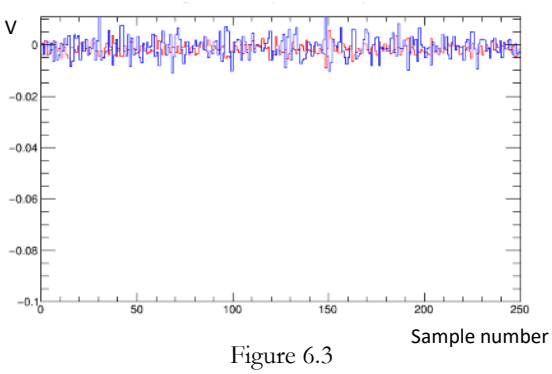

Figure 6.3

Traces for 1M Ω and 15pF
on bottom board and
1M Ω and 6.8pF on top board

6.2. Averaging and normalisation:

The traces were averaged and normalized as explained in section 4.2.1. The blue traces represent the bottom board signals and the red traces represent the top board traces. The x-axis shows the sample number whereas the y-axis shows the amplitude of the signal in mV.

Figure 6.4 shows the averaged and normalized traces for the initial resistor capacitor values with which the board was designed. Here, the maximum amplitude of the peak is close to 0.55 mV and there is also an undershoot of -0.2 mV just after the peak. Both these peaks are reduced in Figure 6.5 with the amplitude at 0.47mV and almost no undershoot. The signal in Figure 6.4 is also very short and fast compared to Figure 6.5. This may be due to the small resistance value used. More noise peaks can be observed in Figure 6.5. It has to be noted that due to the normalisation condition the actual peak heights are affected by the signal shape and the noise level, which in turn depends on the number of traces that have been averaged. The curves are unbiased estimates for the average signal shape and thus provide valuable information. The absolute peak values, however, are only indicative and should not be used in quantitative comparisons. Here the results from the event based analysis are authoritative.

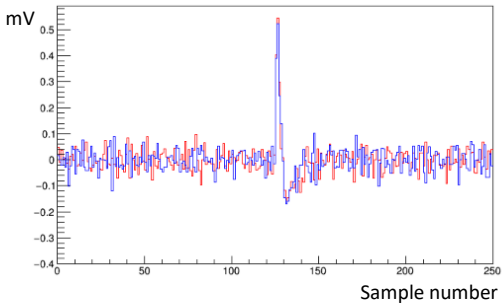

Figure 6.4
Averaged and normalised traces for 1MΩ and 10pF

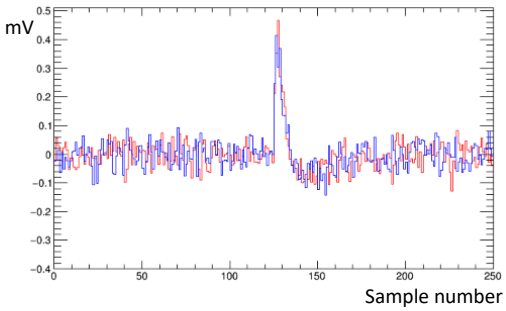

Figure 6.5
Averaged and normalised traces for 10MΩ and 10pF

Upon replacing the resistors with a higher value of 20 MΩ, better traces as compared to Figure 6.4 are observed due to the increased signal width. The upper peak is at around 0.4 mV while the undershoot is reduced significantly, and much less noise is also observed. The 47M Ω and 15pF from Figure 6.7 show a similar trace with almost the same voltage peak at around 0.4 mV. Interestingly, the signal width in Figure 6.7 is slightly bigger than Figures 6.5 and 6.6. Thus one can see that the signal width increases slightly with increase in the resistor value.

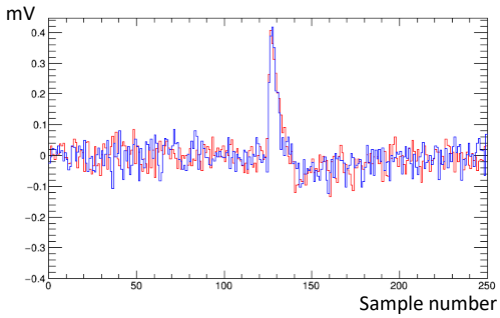

Figure 6.6
Averaged and normalised traces for 20MΩ and 10pF

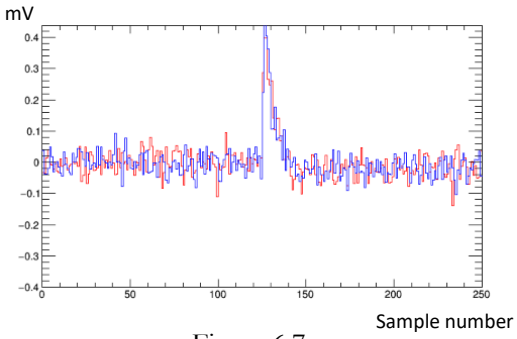

Figure 6.7
Averaged and normalised traces for 47MΩ and 15pF

The averaged traces for the special case with a foil in between the boards shown in Figure 6.8 yield poor results for the bottom board (blue trace), give almost no output signal and the top board (red trace), and display a higher amplitude in both directions. Figure 6.9 shows a much poorer signal on both boards with increased noise too.

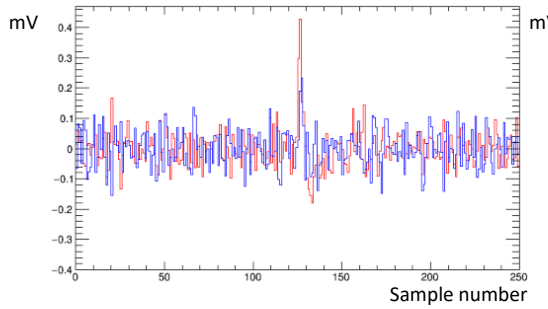

Figure 6.8
Averaged and normalised traces for 1MΩ and 10pF with foil between boards

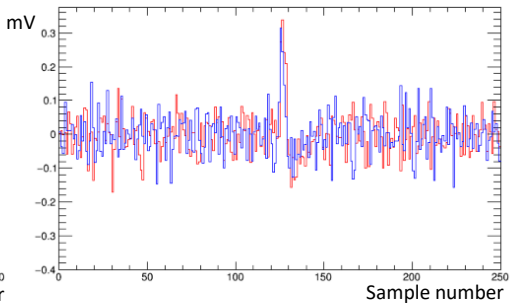

Figure 6.9
Averaged and normalised traces for 1MΩ and 15pF on bottom board and 6.8pF on top board

Thus, from the averaged and normalized traces, the 20MΩ and 10pF combination seems to give the best output signal with a low noise level compared to the signal.

6.3. Scatter plots

The scatter plots were created using a 2D histogram in ROOT, where the y-axis shows 'Fbot', which is the scalar product of the normalized averaged bottom trace with the trace, and the x-axis shows 'Ftop', which is the same for the top board. This plot allows to understand any correlation or anti-correlation between the signal of the boards if any exists. The points are presented as a 2D histogram, with a colour scale to represent the fill state of each bin. The efficiency of the boards was also calculated later on with the help of these scatter plots. Figure 6.10 shows the scatter plot for 1MΩ and 10pF. Here one can see a concentrated disc shape that is dominated by noise. There does not seem to be much coincidence signal which can be discriminated easily. But in Figure 6.11 the coincidences between the boards are nicely separated from the noise.

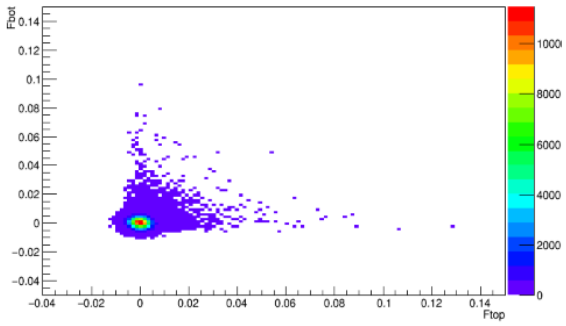

Figure 6.10
Scatter plot for 1MΩ and 10pF

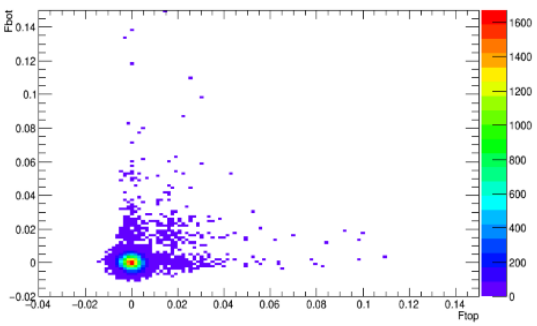

Figure 6.11
Scatter plot for 10MΩ and 10pF

The scatter plot for 20MΩ and 10pF showed a comparatively better result than with other resistor-capacitor combinations and can be seen in Figure 6.12. It looks much better than earlier figures and much more coincidences are obtained which can be properly discriminated from the noise. Figure 6.13 shows the plot for 47MΩ and 15pF. The noise here seems much less but this can be due to the 15pF capacitor used, as the noise reduces with the capacitance values, which is discussed in the coming sections. There is however no significant improvement in the number of coincidences obtained.

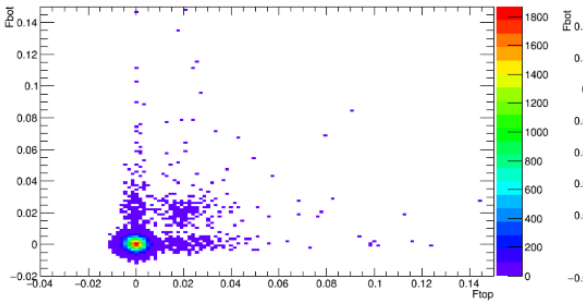

Figure 6.12
Scatter plot for 20MΩ and 10pF

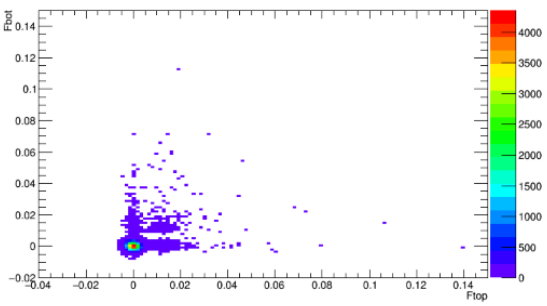

Figure 6.13
Scatter plot for 47MΩ and 15pF

The scatter plots for 100MΩ and 10pF too did not yield good results and are included in the Appendix along with the plots for other resistor-capacitor combinations. In the Figure 6.14, for a foil between the boards, one can see that there are almost no coincidence between the boards, with signals only on the top board, and significant noise on the bottom board. A similar trend can be seen for the Figure 6.15 having a horizontal oval shape for the noise, very few coincidence candidates and very little signal on either board.

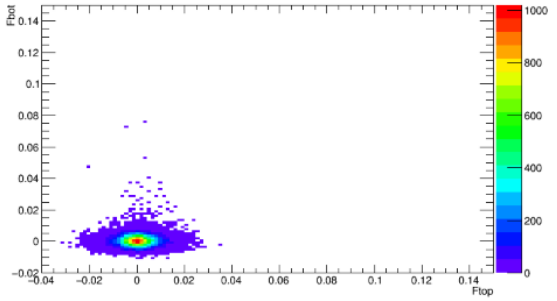

Figure 6.14
Scatter plot for 1MΩ and 10pF with foil between boards

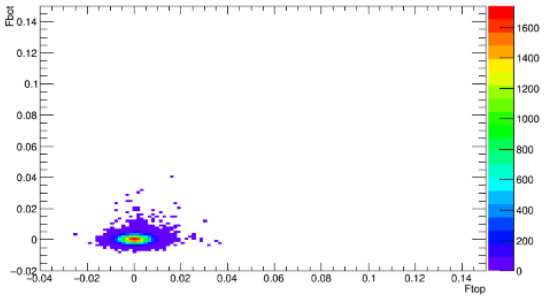

Figure 6.15
Scatter plot for 1MΩ and 15pF on bottom board and 6.8pF on top board

6.4. Special analysis:

During the analysis, a reading was taken for 10MΩ and 6.8pF that resulted in output with almost no signal. Additional readings with earlier successful combinations like 10MΩ with 10pF and also with 15pF, also resulted in very bad data sets, suggesting that there was a problem in the board design that did not exist earlier. This was initially suspected to be from timing jitters, and in order to analyse the issue, plots which show the location of the maximum for each trace in time were decided to be examined for any jitter. Along with this, the noise levels over time was also decided to be inspected.

6.4.1. Problem rectification:

The location of the maxima was plotted for the test data taken. This allowed us to determine any timing jitter between the trigger system and the diode data, which could impact the data.

For the noise analysis, the standard deviation of the signal values of the traces were calculated and plotted against the measurement time as recorded in the filenames of the datafiles recorded for each event.

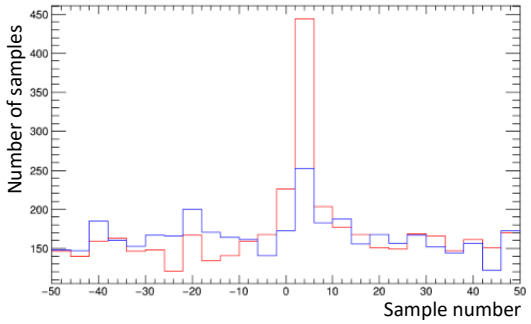

Figure 6.16
Maxima plots for 10MΩ and 6.8pF faulty traces

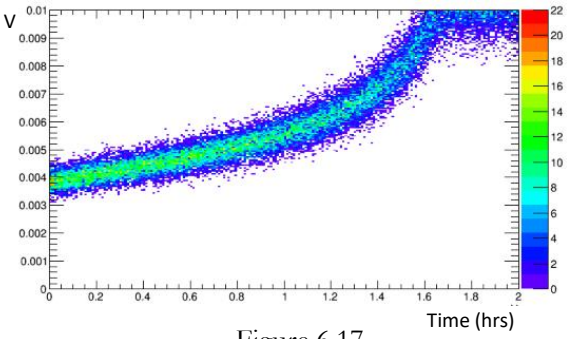

Figure 6.17
Noise level for 10MΩ and 6.8pF faulty bottom board

Figure 6.16 shows the problematic readings of 10MΩ and 6.8pF where we can see that the blue trace of the bottom board signal is almost not showing any signal. This implies that there is a defect on the bottom board. However, these plots show no timing jitter. Hence, the timing of the triggering system works correctly.

From Figure 6.17 we observe an increase in the noise level with time, which is a trend that should not exist in the measurement. This shows that there might be a faulty component or loose contact on the board which contributes to extra noise. While testing the connections, a short circuit was thought to have occurred, but this was caused by the batteries being inserted during the testing with the multimeter. Hence, this was not a problem. Also, the normal wire-connectors then used to connect both the boards seemed to have a loose contact. This was re-soldered.

Upon testing the board, the AD8628 on the bottom board was found to be damaged and had to be replaced with a new one. Additionally the connectors which connect the board to the oscilloscope were found to get loose over time which explains the increase in noise over time in the Figure 6.17. This was fixed by improving the soldering connection. Upon rectifying these problems, the detector began to function well as earlier. The noise levels and the maxima plots after rectifying the problem is shown in Figure 6.18 and Figure 6.19 respectively.

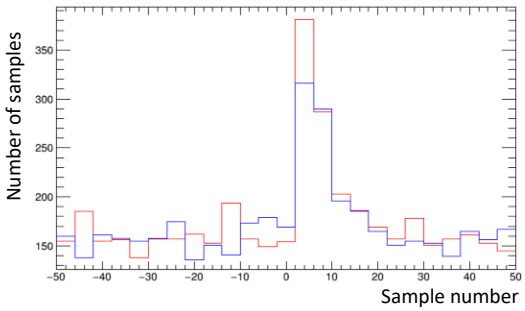

Figure 6.18
Maxima plots for 10MΩ and 6.8pF rectified

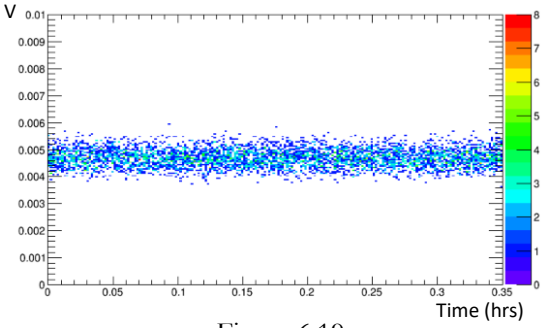

Figure 6.19
Noise level for 10MΩ and 6.8pF bottom board rectified

6.4.2. Maxima and noise analysis

The maxima plots and noise levels were also plotted later for other readings too to understand any jitter if present. Unlike the earlier numbering of the bins which was from 1 to 250, here a different numbering from -124 to 125 was used such that the expected trigger point is at 0.

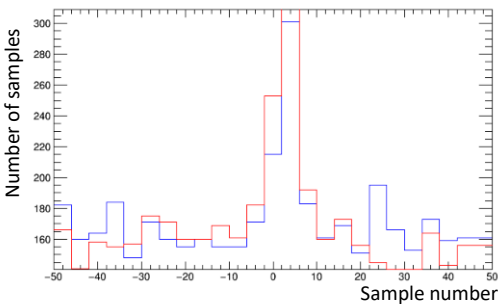

Figure 6.20
Maxima plots for 1MΩ and 10pF

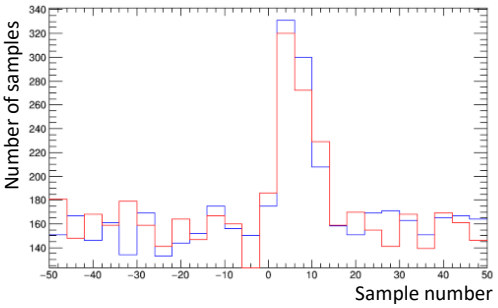

Figure 6.21
Maxima plots for 10MΩ and 10pF

In Figure 6.20 both the bottom and top board signal can be observed to rise almost instantly after the 0 point, which is the trigger point and they also fall without much delay. Similar trend can be observed in Figure 6.21 with both the top and bottom boards responding similarly.

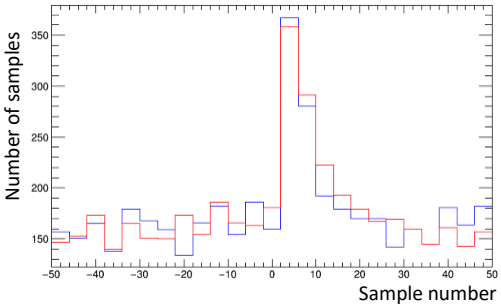

Figure 6.22
Maxima plots for 20MΩ and 10pF

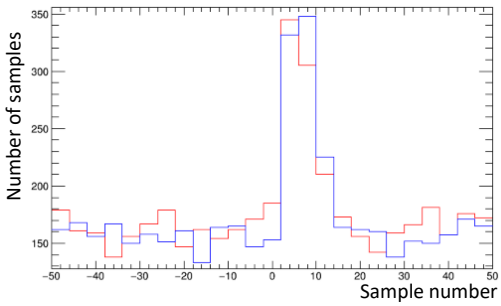

Figure 6.23
Maxima plots for 47MΩ and 15pF

Both Figures 6.22 and 6.23 show lesser signals before the trigger and comparatively higher signal just after the trigger point. No jitter is observed in these cases. Figure 6.24 shows that the foil placed in between boards does not yield any good output and the figure 6.25 too shows poor results as compared to the others.

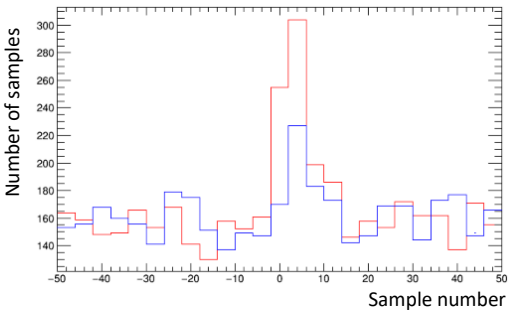

Figure 6.24
Maxima plots for 1MΩ and 10pF
with foil between boards

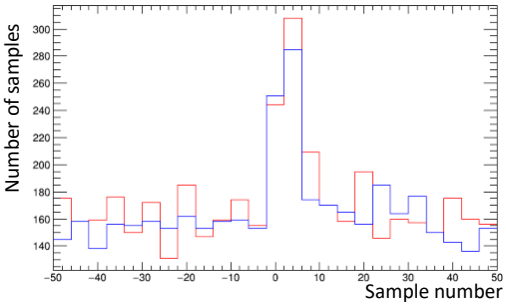

Figure 6.25
Maxima plots for 1MΩ and 6.8pF on
top board and 15pF on bottom board

From the maxima plots, one can see that there is no jitter issue with the boards. Moreover, the plots indicate that a foil between the boards does not provide a good working setup, neither does the use of different capacitors on the two boards. The noise levels were calculated for all the earlier samples too.

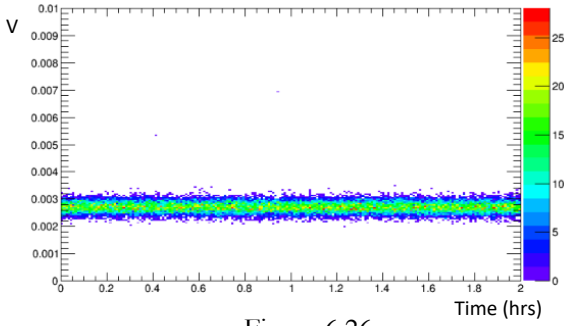

Figure 6.26
Noise level for 20MΩ and 10pF

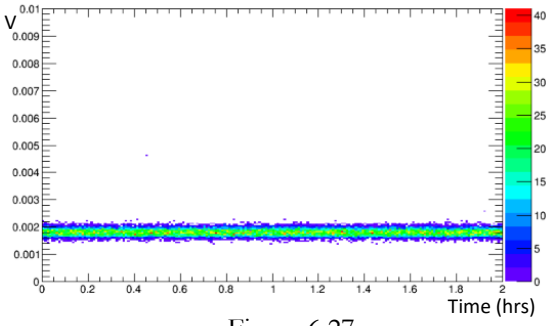

Figure 6.27
Noise level for 20MΩ and 15pF

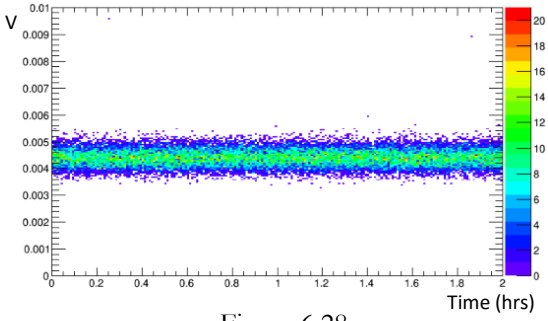

Figure 6.28
Noise level for 20MΩ and 6.8pF

It was observed that, irrespective of the resistor value, the noise level mainly depends on the capacitor value. When 6.8pF is used, the noise level is about 4 to 5 mV, when 10pF is used, the noise level is about 3 mV and when 15pF is used, the noise level is at 2 mV. An example is shown in Figure 6.26 to 6.28. A compilation of noise measurements is shown in Figure 6.37.

In order to understand whether a reduction in the number of diodes will contribute to a better signal and reduced noise, 40 diodes were disconnected from both the boards, with only 10 diodes in a row now remaining connected. 20MΩ and 10pF was used for testing. Figure 6.29 shows the scatter plot obtained for this configuration, from which one can see that there are almost no coincidences and the noise level is not much reduced as seen in Figure 6.30.

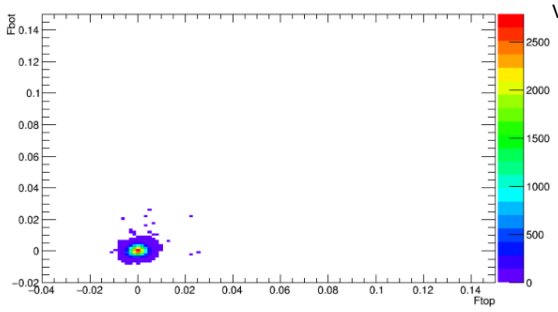

Figure 6.29
Scatter plot for 20MΩ and 10pF with 10 diodes

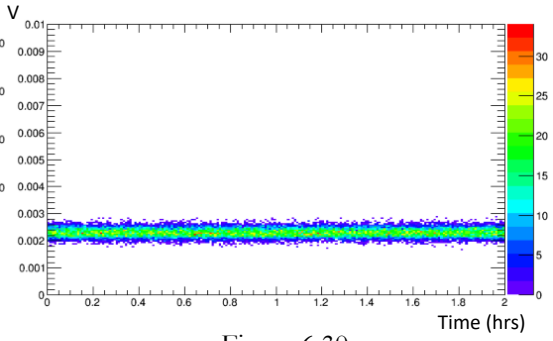

Figure 6.30
Noise level for 20MΩ and 10pF with 10 diodes.

Upon increasing the number of diodes to 20 on each board, the coincidence rate between the boards does improve slightly as seen in Figure 6.31, but not a visibly higher change in the noise level which is shown in Figure 6.32.

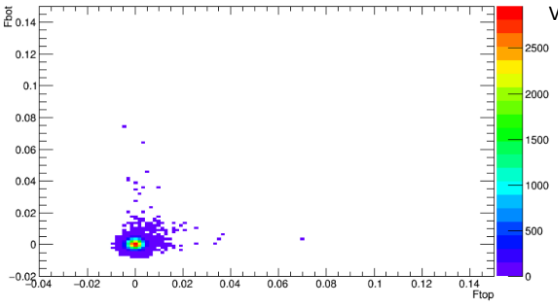

Figure 6.31
Scatter plot for 20MΩ and 10pF with 20 diodes

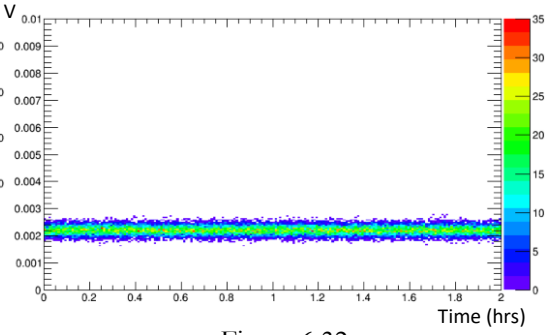

Figure 6.32
Noise level for 20MΩ and 10pF with 20 diodes.

During these measurements, even though the other diodes are disconnected, they are still on the board which, by parasitic couplings, may contribute to an increased noise. Thus the idea of short circuiting the other diodes so that they don't provide any kind of signal to the rest of the circuitry was considered. This gives a marginally reduced noise level as shown in Figure 6.34, but unfortunately in almost no coincidence which can been seen in Figure 6.33.

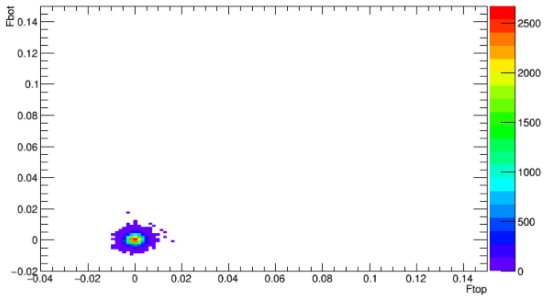

Figure 6.33
Scatter plot for 10MΩ and 10pF with 10 diodes and rest shorted.

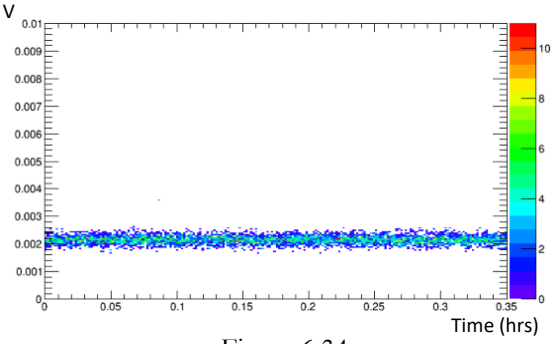

Figure 6.34
Noise level for 10MΩ and 10pF with 10 diodes and rest shorted.

Now even though the diodes are short circuited, they are still on the board, hence measurements were also taken by removing the disconnected diodes from both the boards. This resulted in a significantly reduced noise but very low coincidence rates.

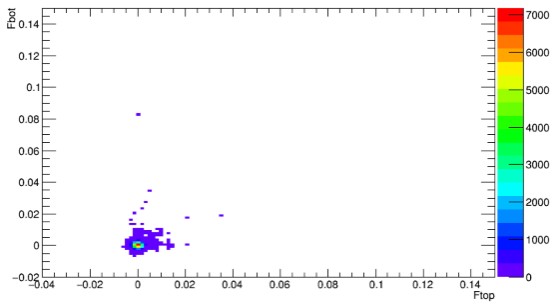

Figure 6.35
Scatter plot for 20MΩ and 10pF with 10 diodes and 40 removed.

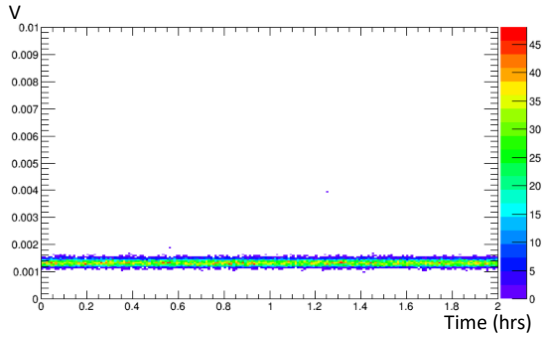

Figure 6.36
Noise level for 20MΩ and 10pF with 10 diodes and 40 removed.

From all the readings taken above, we do see a relation between the capacitance and the noise levels, with the noise level increasing with decreasing capacitance. In order to understand this better, a comparison of the noise levels of all the measurements of both top and bottom board was conducted and the results were obtained as shown in Figure 6.37.

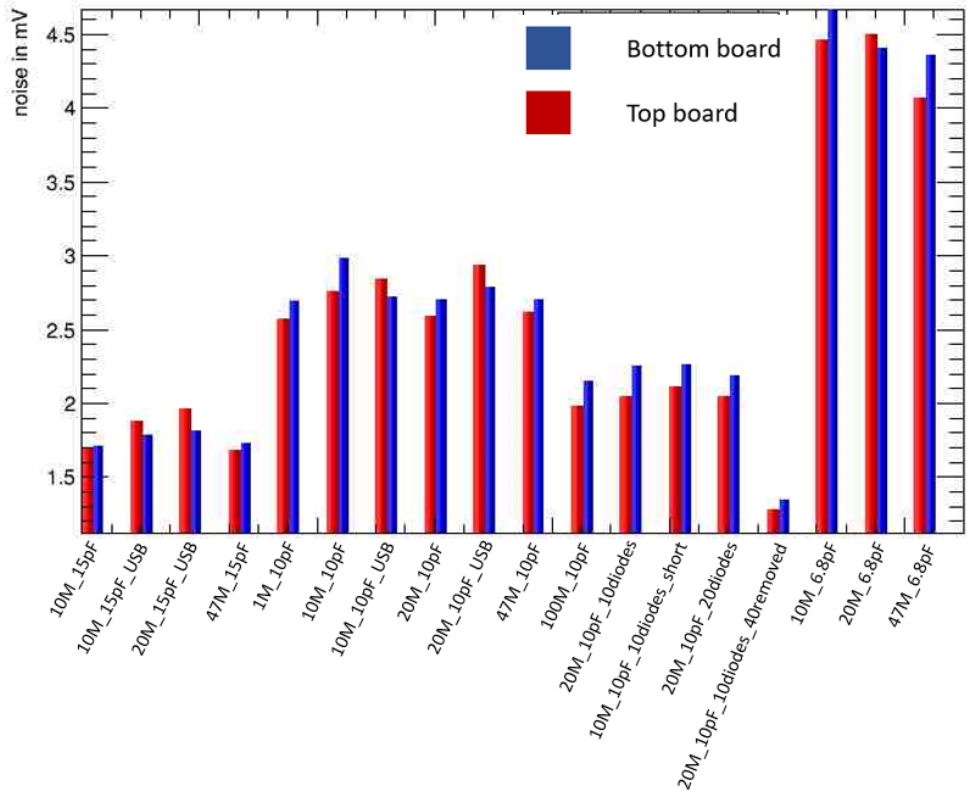

Figure 6.37

Noise level comparison for all major measurements.

6.5. Efficiency

Table 6.1 shows various parameters calculated in the above section, for various resistor-capacitor combinations. Few readings were taken with a normal 12V battery supply whereas few where taken with the help of USB supply. The readings for 10 diodes, 20 diodes, 10 diodes with the rest shorted and also for 10 diodes with 40 diodes removed are also compared with these values. With the help of a Monte Carlo simulation, the geometric parameters were obtained, as mentioned in section 4.2.3.1. The acceptance probabilities obtained from the simulation were:

between two scintillators: 83.63%

bottom board and scintillators: 91%

top board and scintillators: 92%

both boards and scintillators: 47%

Slightly different geometric parameters were obtained for the measurements with USB and those with a 12V supply. This was due to the different distances that the board was placed from the scintillators during these measurements. the values obtained were:

USB measurements: $g_{13} = g_{23} = 0.01090$, $g_{123} = 0.00569$

non-USB measurements: $g_{13} = g_{23} = 0.01091$, $g_{123} = 0.00548$

Average-based analysis:

From the scatter plot the coincidence counts are calculated for bottom board with the scintillators, top board with the scintillators, both boards with the scintillator and also no coincidence, too, as mentioned in section 4.2.3.2. The obtained counts are C_1, C_2, C_{12} and 'noise' respectively. Equation (20) in section 4.2.3.2 gives the efficiency of the individual boards.

The efficiency as obtained from the scatter plot is as shown in Table 6.1.

S.no	R	C	No. of events	ε_1	ε_2	$\bar{\varepsilon}$	note
1.	1MΩ	10pF	225811	0.414	0.419	0.473	12V supply
2.	10MΩ	6.8pF	44935	0.728	0.804	0.825	12V supply
3.	10MΩ	10pF	195732	0.873	0.917	0.933	12V supply
4.	10MΩ	10pF	14341	0.738	0.724	0.720	USB supply
5.	10MΩ	15pF	178830	0.862	0.860	0.928	12V supply
6.	20MΩ	6.8pF	45019	0.921	0.872	0.920	12V supply
7.	20MΩ	10pF	179740	0.865	0.863	0.917	12V supply
8.	20MΩ	10pF	44422	0.913	0.958	0.899	USB supply
9.	20MΩ	15pF	44943	0.886	0.871	0.772	USB supply
10.	20MΩ	10pF	44952	0.587	0.502	0.375	20 diodes
11.	20MΩ	10pF	193320	0.362	0.261	0.637	40 diodes removed

Table 6.1
Efficiency from scatter plot

Table 6.1 gives the efficiencies of few important measurements that were taken. Here we can see that the 10MΩ with 10pF and 15pF show high efficiencies and also the 20MΩ with 6.8pF and 10pF. But since the scores here are calculated using cuts that are manually defined, accurate results are not obtained. Moreover, cuts are difficult to define in the case of data which show poor scatter plots. Hence the event based approach seems more reliable. This can be observed in Table 6.2 and Table 6.3.

Event-based analysis:

S.no	R	C	No. of events	RMS width w_1 (samples)	RMS width w_2 (samples)	Total signal S_1 (V)	Total signal S_2 (V)	Signal to noise ratio S_1/N_1	Signal to noise ratio S2/N2	note
1.	1MΩ	10pF	225811	1.131	1.155	0.040	0.037	6.225	6.114	12V supply
2.	10MΩ	6.8pF	44935	1.903	1.975	0.117	0.105	7.487	7.175	12V supply
3.	10MΩ	10pF	195732	2.141	2.266	0.073	0.074	7.143	7.602	12V supply
4.	10MΩ	10pF	14341	1.183	1.265	0.036	0.045	6.908	7.816	USB supply
5.	10MΩ	15pF	178830	2.339	2.473	0.048	0.050	7.622	7.696	12V supply
6.	20MΩ	6.8pF	45019	2.182	2.244	0.130	0.137	8.149	8.376	12V supply
7.	20MΩ	10pF	179740	2.383	2.499	0.082	0.082	8.378	8.519	12V supply
8.	20MΩ	10pF	44422	2.373	2.426	0.129	0.081	11.926	7.957	USB supply
9.	20MΩ	15pF	44943	2.470	2.550	0.052	0.054	7.909	7.889	USB supply
10.	20MΩ	10pF	44931	1.283	1.369	0.044	0.046	8.261	7.950	10 diodes
11.	20MΩ	10pF	194780	1.316	1.412	0.045	0.044	8.400	7.727	20 diodes
12.	10MΩ	10pF	44471	1.105	1.278	0.036	0.038	7.356	6.850	10 diodes shorted
13.	20MΩ	10pF	193320	1.301	1.402	0.039	0.045	10.826	10.727	40 diodes removed

Table 6.2
Signal to noise ratio results

In an event based analysis, the counts for coincidence are easier to decide as mentioned in section 4.2.3.3. Once the counts are obtained, the efficiencies are found using equation (31) in section 4.2.3.3.

S.no	R	C	No. of events	Noise N_1 (V)	Noise N_2 (V)	C_1	C_2	C_{12}	G	ε_1	ε_2	$\bar{\varepsilon}$	note
1.	1MΩ	10pF	225811	0.0026	0.0025	876	1004	167	0.023	0.355	0.408	0.360	12V supply
2.	10MΩ	6.8pF	44935	0.0044	0.0046	427	466	210	0.021	0.870	0.951	0.906	12V supply
3.	10MΩ	10pF	195732	0.0029	0.0027	1954	1972	931	0.021	0.915	0.924	0.914	12V supply
4.	10MΩ	10pF	14341	0.0021	0.0021	138	115	60	0.018	0.887	0.736	0.857	USB supply
5.	10MΩ	15pF	178830	0.0017	0.0017	1896	2001	835	0.025	0.972	1.025	0.905	12V supply
6.	20MΩ	6.8pF	45019	0.0044	0.0044	389	478	208	0.019	0.793	0.974	0.900	12V supply
7.	20MΩ	10pF	179740	0.0026	0.0026	1872	1962	822	0.025	0.955	1.000	0.896	12V supply
8.	20MΩ	10pF	44422	0.0028	0.0027	458	439	209	0.021	0.946	0.906	0.908	USB supply
9.	20MΩ	15pF	44943	0.0019	0.0017	390	377	163	0.020	0.796	0.769	0.798	USB supply
10.	20MΩ	10pF	44931	0.0201	0.0220	86	92	34	0.005	0.176	0.192	0.364	10 diodes
11.	20MΩ	10pF	194780	0.0020	0.0020	778	768	377	0.008	0.366	0.361	0.582	20 diodes
12.	10MΩ	10pF	44471	0.0021	0.0022	86	76	30	0.004	0.177	0.156	0.344	10 diodes shorted
13.	20MΩ	10pF	193320	0.0012	0.0013	392	405	177	0.004	0.186	0.192	0.400	40 diodes removed

Table 6.3
Efficiency from event based analysis

From Table 6.3, we can see that there are a few measurements that have efficiencies slightly above unity. This can be attributed to the setup being slightly changed for each measurements due to certain systematic uncertainties like the position of the diodes both in x and y direction, and this may result in a change in the geometric parameters. Hence this cannot be modelled for each measurement individually. Also statistical fluctuations in the background estimates when determining the coincidence counts play a role. Thus a fluctuation of about one percent can be expected.

When comparing both event based and average based analysis, one can observe that the values in Table 6.1 and Table 6.3 have a difference of about 8% - 10%.

Let us consider the case for 10MΩ and 10pF with 12V supply:

for an average based analysis,

$\varepsilon_1 = 0.873$, $\varepsilon_2 = 0.917$, $\bar{\boldsymbol{\varepsilon}} = 0.933$

for an event based analysis,

$\varepsilon_1 = 0.915$, $\varepsilon_2 = 0.924$, $\bar{\boldsymbol{\varepsilon}} = 0.914$

Here, only for the bottom board do we see a difference of 4.2 % whereas the others are close to the same. A similar trend can be observed in most of the measurements. This can be due to the fact that the average based analysis utilizes the method of using cuts that are defined by simply looking at the scatter plots with the naked eye. Changing the cuts can significantly change the count number. Also, the shape of the cut can affect the count number, i.e. here a simple horizontal and vertical cut is used but scatter plots have coincidences which are not strictly well defined and thus using diagonal cuts may help improve the count.

Overall, the readings of 10MΩ with 6.8pF, 10pF(with 12V supply) and 15pF and 20MΩ with 10pF (with USB as well as 12V supply) give good efficiencies. Upon comparing the signal to noise ratios, the 20MΩ and 10pF seems to perform slightly better than rest. Thus, the 20MΩ and 10pF was decided to be used in the final detector design.

Chapter – 7
Comparison with SILEX version 2

The design values used for version 2 board was 10MΩ and 6.8pF. Hence a comparison of the measurements obtained from the same values on the version 3 board will give the required result.

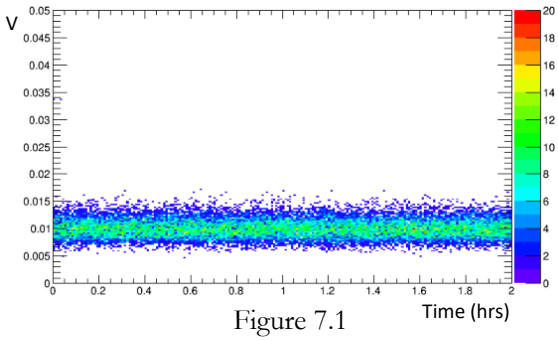

Figure 7.1
Noise level for version 2

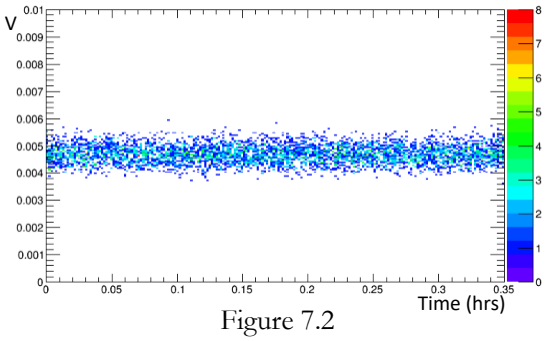

Figure 7.2
Noise level for version 3

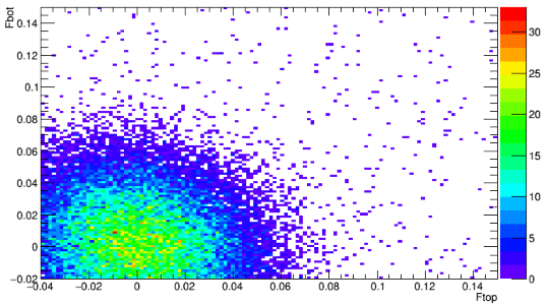

Figure 7.3
scatter plot for version 2

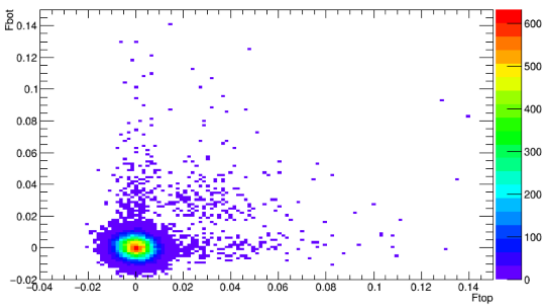

Figure 7.4
scatter plot for version 3

When comparing the noise levels for both versions, the noise level for version 2 as seen from Figure 7.1 is much higher than its version 3 counterpart. Figure 7.1 shows a noise level of around 10mV and Figure 7.2 shows approximately 4 to 5 mV. This is a significant decrease to almost half its earlier value. When looking at the scatter plots, Figure 7.3 shows quite a lot of noise and very few coincidences, while Figure 7.4 of the version 3 shows less noise and much better separated coincidence counts. The signal to noise ratio of the version 2 board was also found to be 4.0062 and 3.8996 for bottom and top boards respectively, while the same for version 3 was 8.3077 and 7.1757 respectively. This hence proves that the version 3 detector boards have much better performance.

Chapter – 8

Conclusion

Upon conducting various analysis on the Silex version 3 detector, it can be concluded that the version 3 detector shows much better performance and reduced noise than its previous version. The critical parameters like noise, signal to noise ratio, signal coincidence and efficiency were analysed which helped in the optimization of the design. The event based analysis does prove to be a better analysis technique than the average based one, due to the less well defined cut criteria of the latter, which hence provides a comparatively less reliable result. In an event based calculation, the actual background of the current event is considered and this method is more robust since the detector is even allowed to slowly change with time, unlike in average based analysis where any change in the detector can cause a significant change in the results. From the analysis conducted, the 20MΩ and 10pF in the amplifier design gave really good results. In the future, work can be done such that the detector output can be sent to a microcontroller which can then process the data. The event based analysis is also less computing intensive, which makes it better suited for implementation on a micro-controller. The introduction of a micro-controller allows for more freedom of movement with the detector, along with less power requirements. This will allow the launch of the muon detector as a product that helps students at school and university level to better understand the detection of muons.

References :

[1] https://en.wikipedia.org/wiki/Max_Planck_Institute_for_Nuclear_Physics [Online; accessed 07-07-2020]

[2] https://www.mpi-hd.mpg.de/mpi/de/forschung/ueberblick [Online; accessed 07-07-2020]

[3] https://root.cern/about/ [Online; accessed 07-07-2020]

[4] https://physics.stackexchange.com/questions/208410/how-can-the-unstable-particles-of-the-standard-model-be-considered-particles-in#:~:text=The%20muon%20is%20unstable%20because,in%20about%202%CE%BCs.&text=A%20muon%20weighs20about%20105.7,energies%20of%20all%20the%20particles. [Online; accessed 07-07-2020]

[5] https://apatruno.files.wordpress.com/2016/09/lecture52.pdf [Online; accessed 17-07-2020]

[6] https://gustavus.edu/physics/concertFiles/media/Cosmic_Ray_Muon_Detection_Thesis.pdf [Online; accessed 24-07-2020]

[7] https://uncw.edu/phy/documents/cosmicraymuons.pdf [Online; accessed 24-07-2020]

[8] https://www.vox.com/the-highlight/2019/7/16/17690740/cosmic-rays-universe-theory-science [Online; accessed 17-07-2020]

[9] Observer Experiment for Students" https://arxiv.org/abs/1309.3391v1 **[astro-ph.IM]** [Online; accessed 17-07-2020]

[10] https://www.nbi.dk/~xella/lecture_16Feb2009.pdf [Online; accessed 24-07-2020]

[11] *Detection of the Angular Distribution of cosmic ray muons and Development of a low-cost Silicon Detector*, Hendrik Borras Link : https://pure.mpg.de/pubman/faces/ViewItemOverviewPage.jsp?itemId=item_2573792 [Online; accessed 24-07-2020]

[12] http://cdn.teledynelecroy.com/files/pdf/hdo6000_oscilloscope_datasheet.pdf [Online; accessed 02-08-2020]

[13] https://www.ieee.li/pdf/essay/pin_diode_handbook.pdf [Online; accessed 02-08-2020]

[14] https://www.osram.com/ecat/DIL%20SMT%20BPW%2034%20S/com/en/class_pim_web_catalog_103489/global/prd_pim_device_2219543/ [Online; accessed 24-07-2020]

[15] https://www.analogictips.com/improving-transimpedance-amplifiers-bootstrap/ [Online; accessed 02-08-2020]

[16] https://chartio.com/learn/charts/what-is-a-scatter-plot/ [Online; accessed 02-08-2020]

[17] 33RD INTERNATIONAL COSMIC RAY CONFERENCE, RIO DE JANEIRO 2013 THE ASTROPARTICLE PHYSICS CONFERENCE "CosMO – A Cosmic Muon

[18] Alvarez LW et al. Search for hidden chambers in the pyramids. Science. 1970;167:832-839. DOI: 10.1126/science.167.3919.832

[19] Optimization, an Important Stage of Engineering Design,2010, Todd R. Kelley; *The Technology Tea*

[20] https://core-electronics.com.au/tutorials/oscilloscope-triggers-what-how.html [Online; accessed 02-08-2020]

[21] https://cdn.macom.com/applicationnotes/AG312.pdf [Online; accessed 24-07-2020]

[22] H. Borras, private communication

[23] M. Schmelling, private communication

[24]https://www.desy.de/schule/schuelerlabore/standort_zeuthen/kosmische_teilchen/experimente/cosmo_experiment/index_ger.html [Online; accessed 02-08-2020]

List of tables

List of figures

Appendix

All traces:

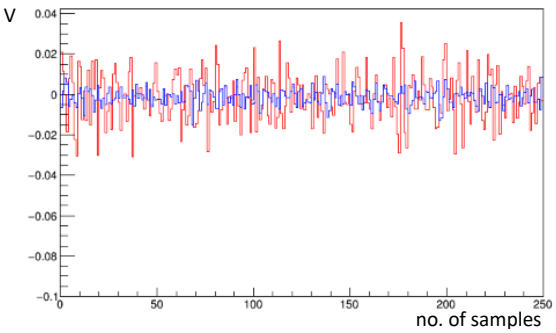

Traces for 1MΩ and 6.8pF

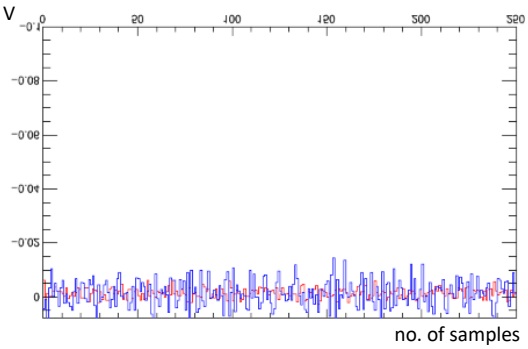

Traces for 1M Ω and 15pF

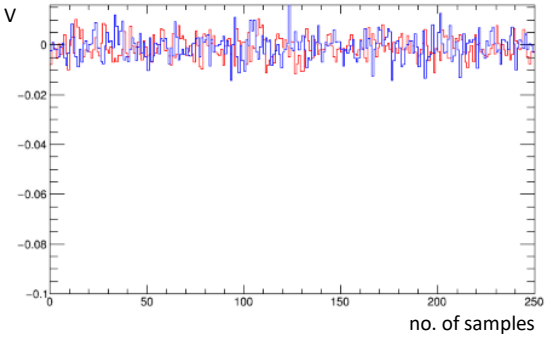

Traces for 10M Ω and 6.8pF

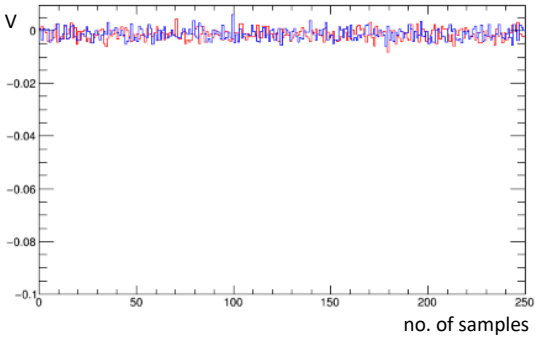

Traces for 10M Ω and 10pF with USB supply

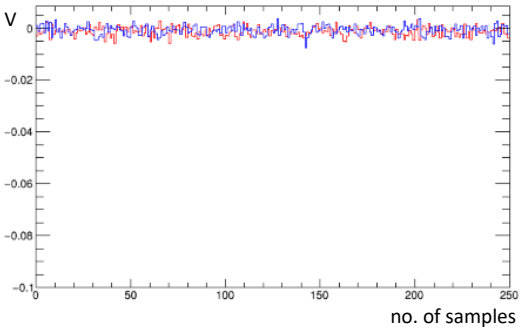

Traces for 10M Ω and 15pF

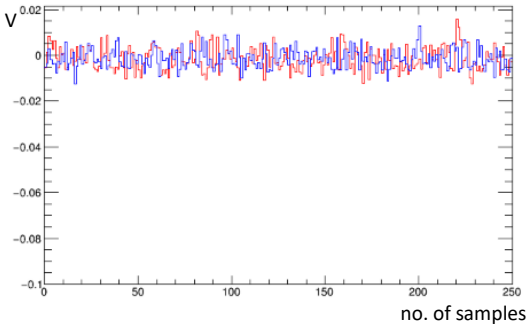

Traces for 20M Ω and 6.8pF

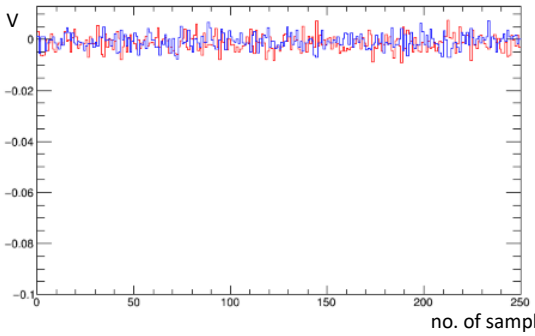

Traces for 20M Ω and 10pF with USB supply

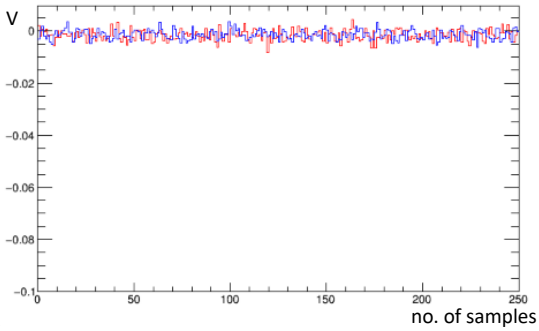

Traces for 20M Ω and 15pF

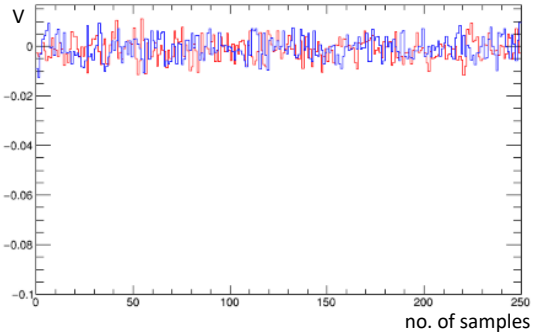

Traces for 47M Ω and 6.8pF

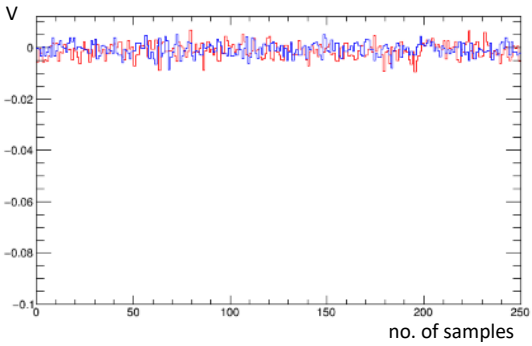

Traces for 47M Ω and 10pF

Averaged and normalized traces:

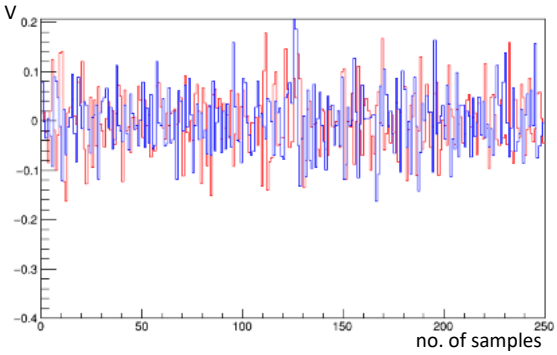

Traces for 1M Ω and 6.8pF

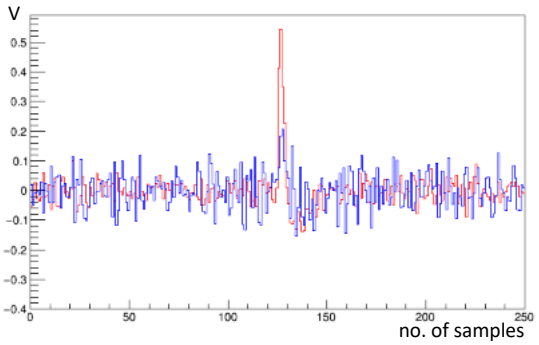

Traces for 1M Ω and 15pF

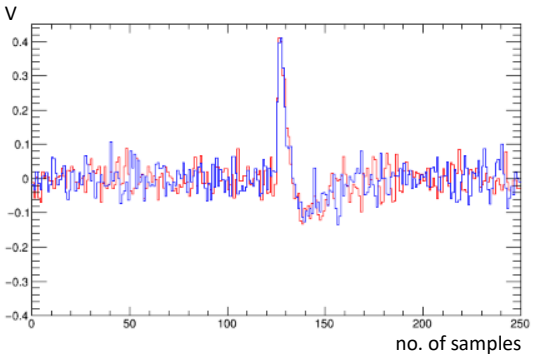

Traces for 10M Ω and 6.8pF

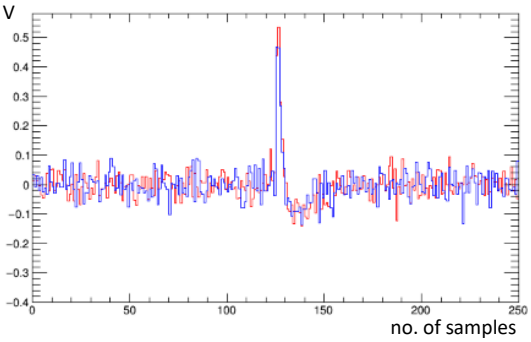

Traces for 10M Ω and 10pF with USB supply

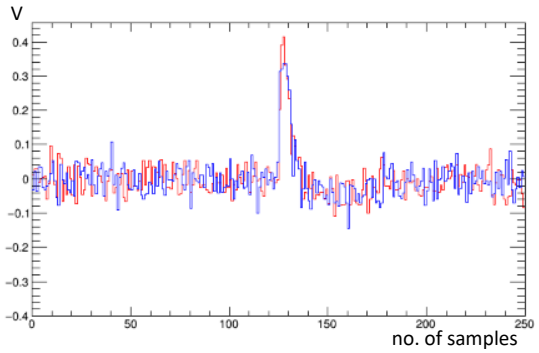

Traces for 10M Ω and 15pF

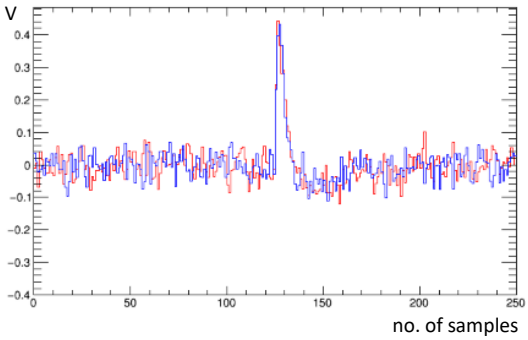

Traces for 20M Ω and 6.8pF

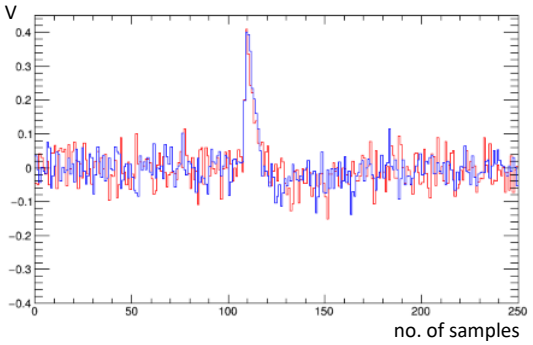

Traces for 20M Ω and 10pF with USB supply

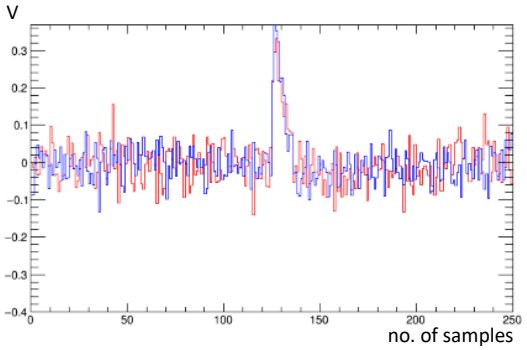

Traces for 20M Ω and 15pF

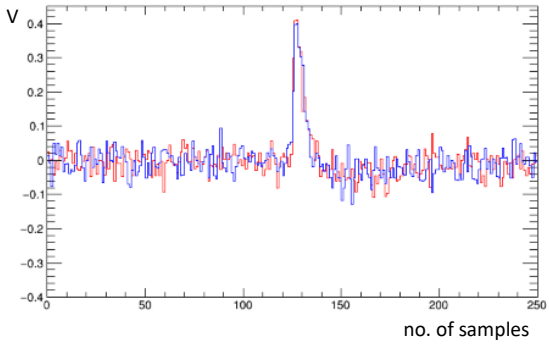

Traces for 47M Ω and 6.8pF

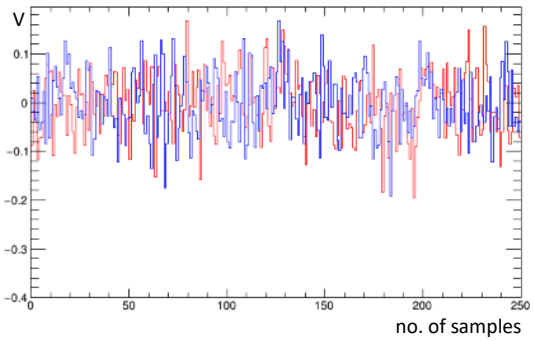

Traces for 47M Ω and 10pF

Maxima plots:

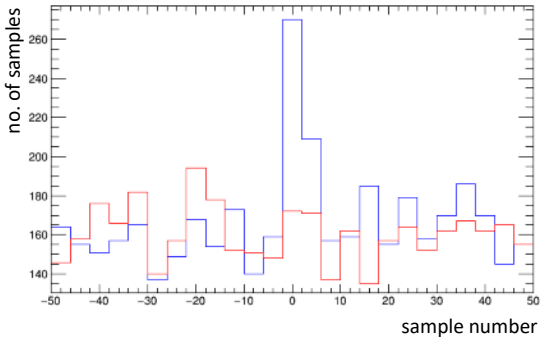

Traces for 1M Ω and 6.8pF

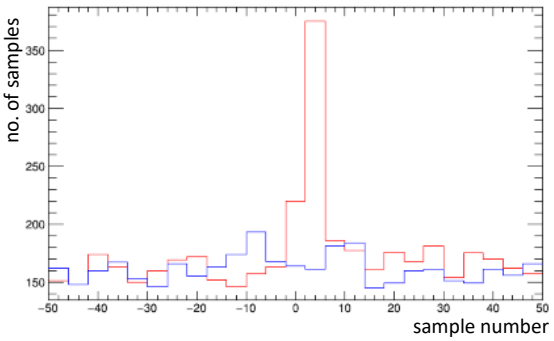

Traces for 1M Ω and 15pF

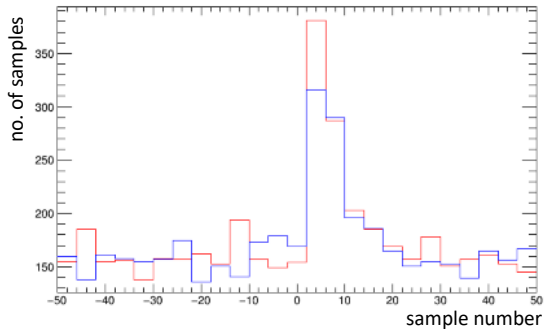

Traces for 10M Ω and 6.8pF

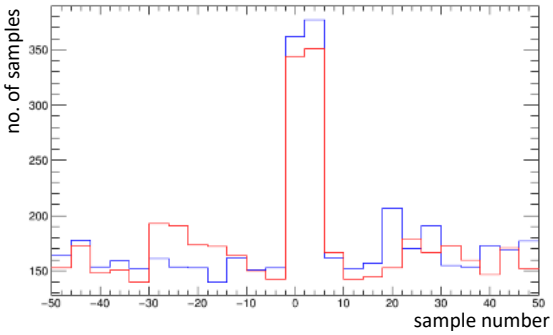

Traces for 10M Ω and 10pF with USB supply

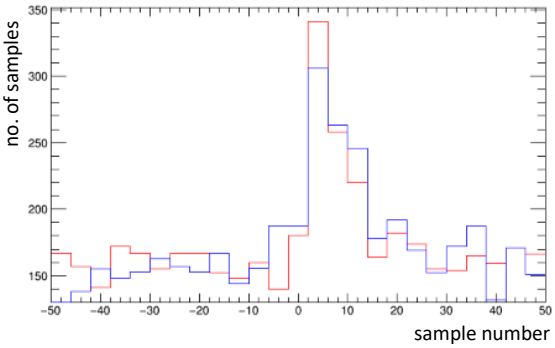

Traces for 10M Ω and 15pF

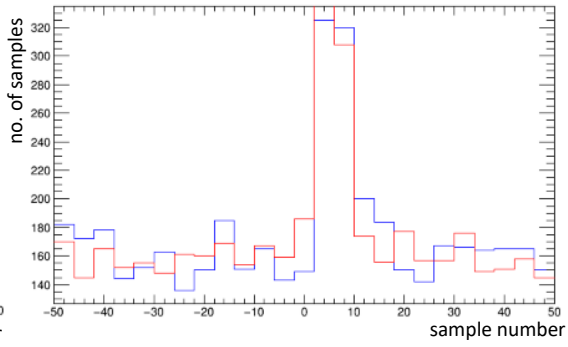

Traces for 20M Ω and 6.8pF

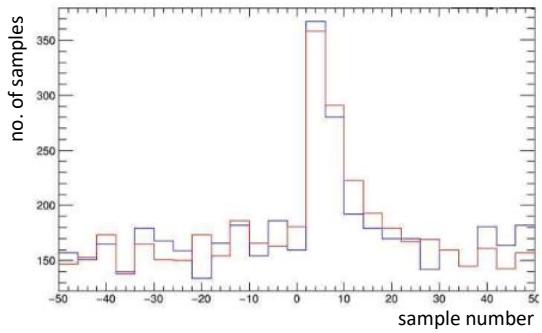

Traces for 20M Ω and 10pF with USB supply

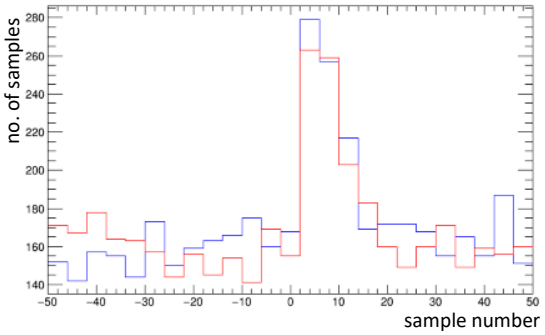

Traces for 20M Ω and 15pF

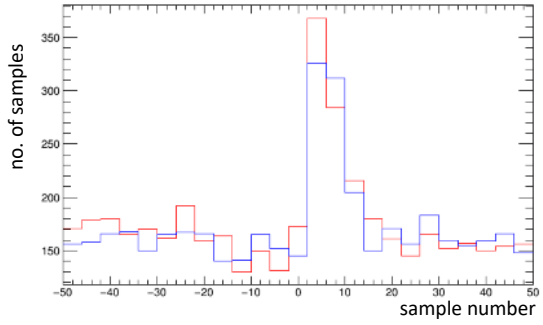

Traces for 47M Ω and 6.8pF

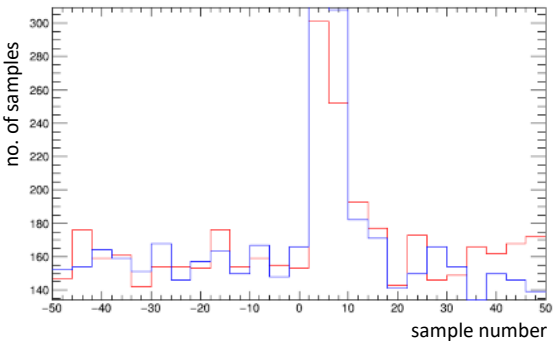

Traces for 47M Ω and 10pF

Scatter plots:

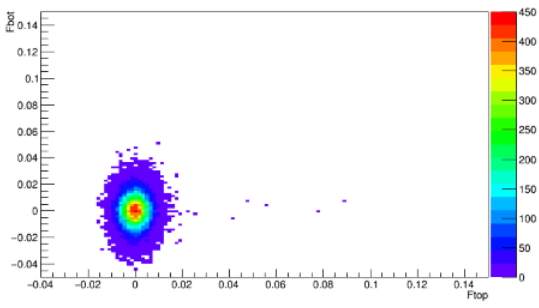

Plots for 1M Ω and 6.8pF

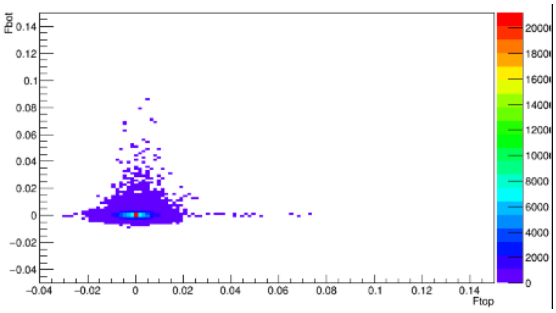

Plots for 1M Ω and 15pF

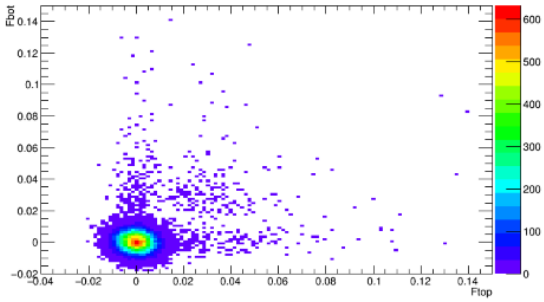

Plots for 10M Ω and 6.8pF

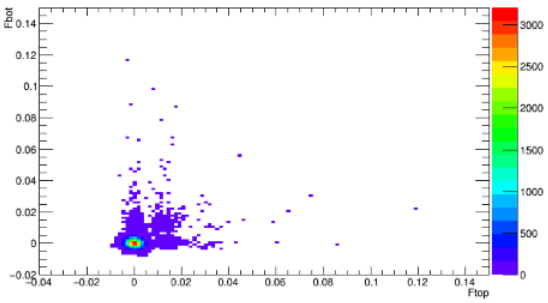

Plots for 10M Ω and 10pF with USB supply

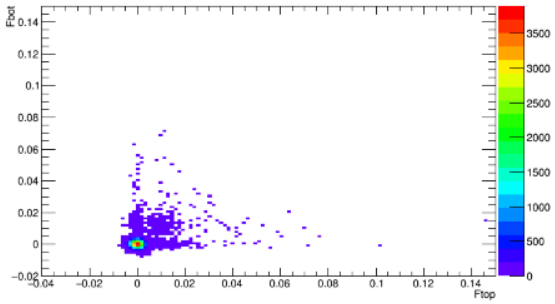

Plots for 10M Ω and 15pF

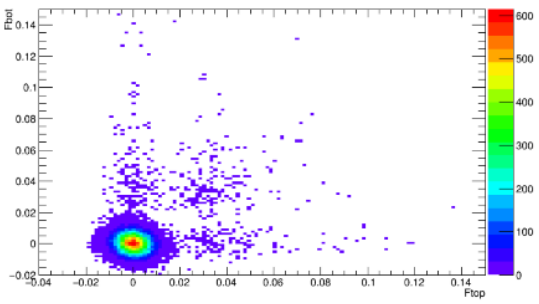

Plots for 20M Ω and 6.8pF

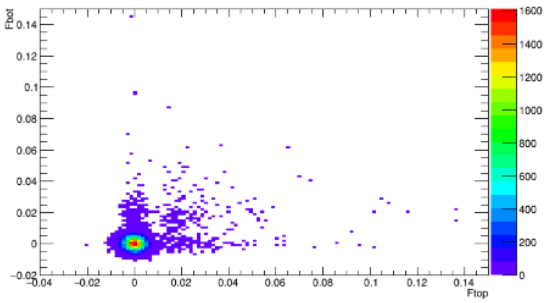

Plots for 20M Ω and 10pF with USB supply

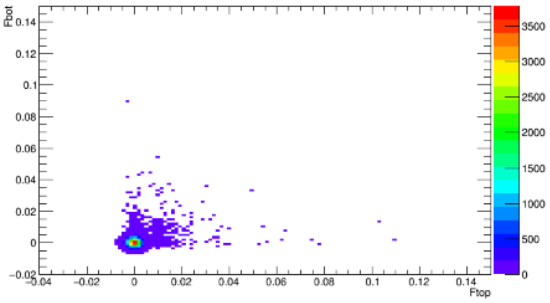

Plots for 20M Ω and 15pF

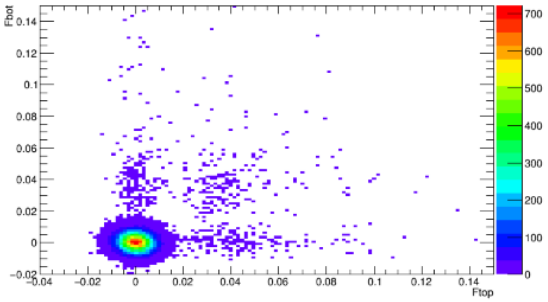

Plots for 47M Ω and 6.8pF

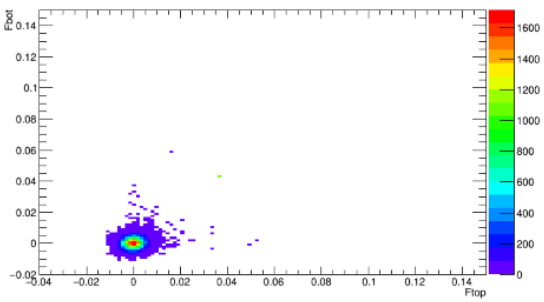

Plots for 47M Ω and 10pF

Noise level:

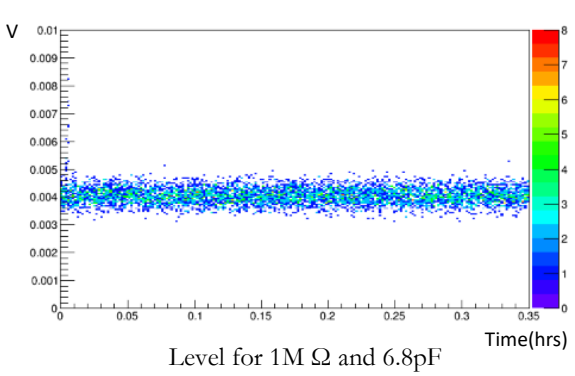

Level for 1M Ω and 6.8pF

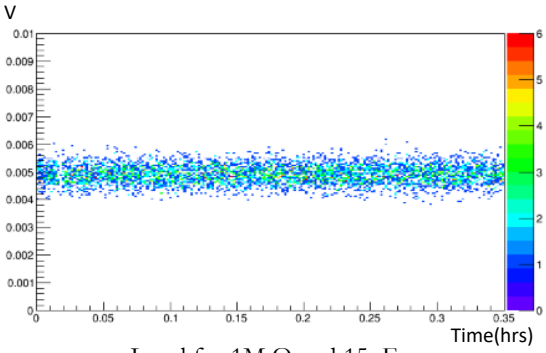

Level for 1M Ω and 15pF

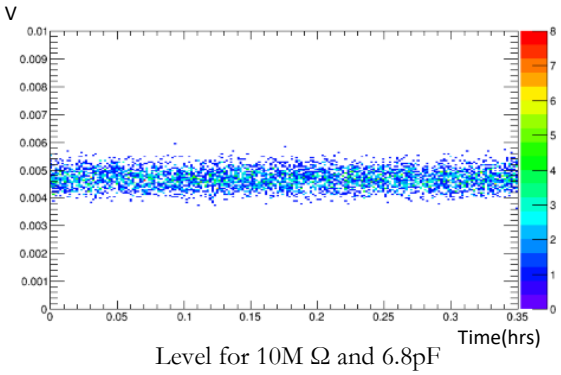

Level for 10M Ω and 6.8pF

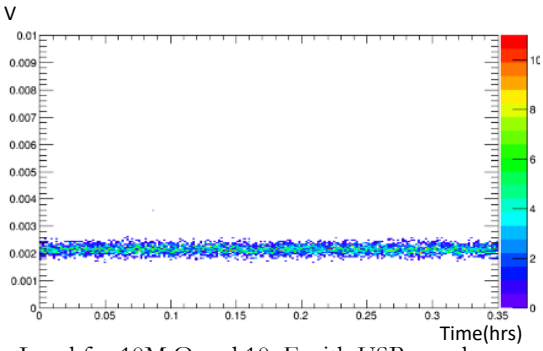

Level for 10M Ω and 10pF with USB supply

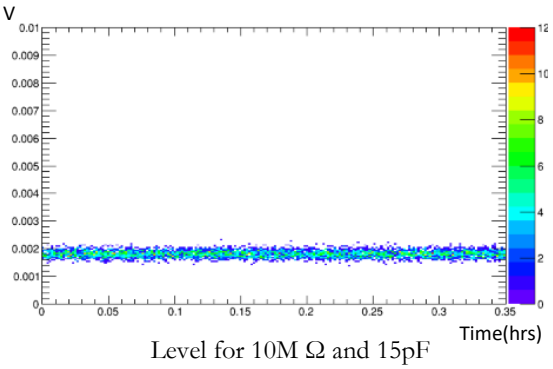

Level for 10M Ω and 15pF

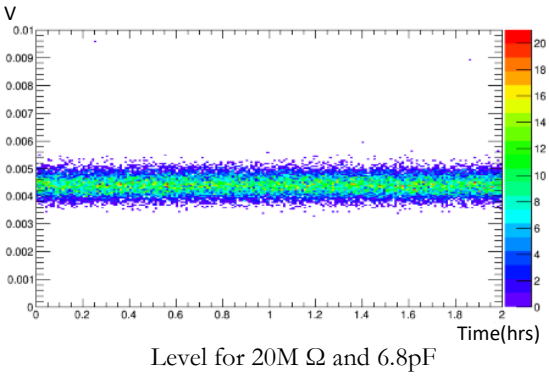

Level for 20M Ω and 6.8pF

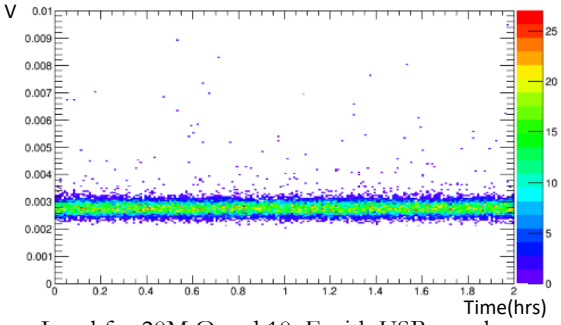

Level for 20M Ω and 10pF with USB supply

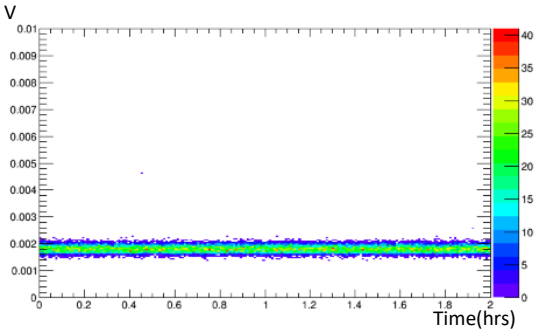

Level for 20M Ω and 15pF

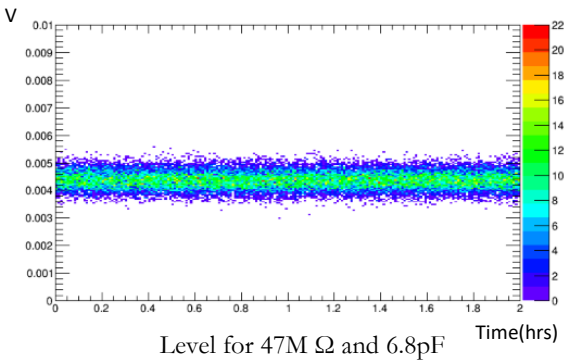

Level for 47M Ω and 6.8pF

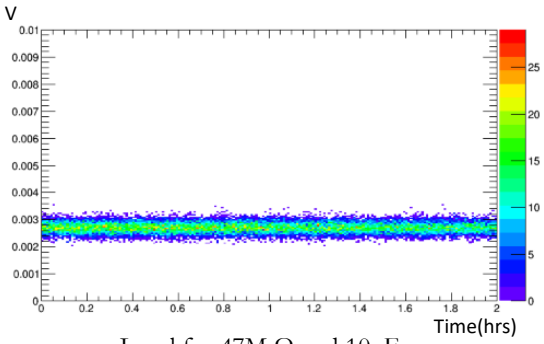

Level for 47M Ω and 10pF

SILEX version 2 traces analysis:

traces with trigger on CosMo detector:

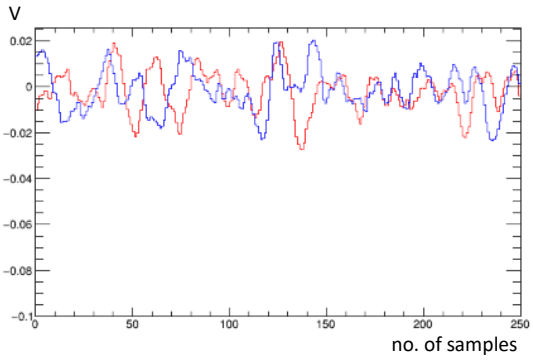

Output traces

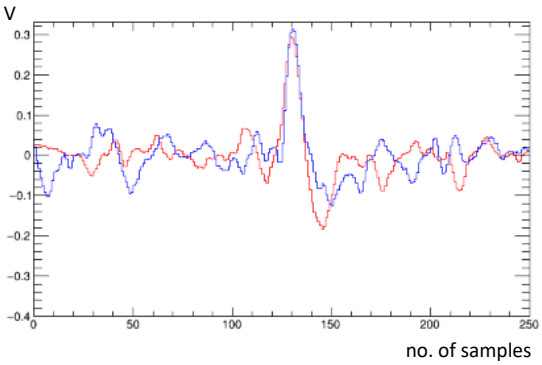

averaged and normalized traces

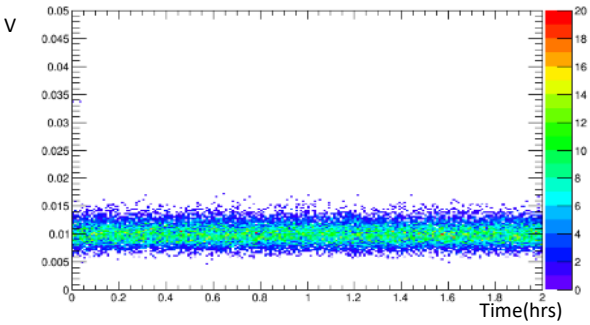

Noise level

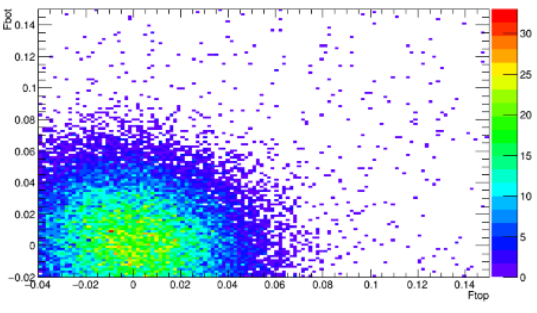

scatter plot

traces with trigger of 0mV on bottom board:

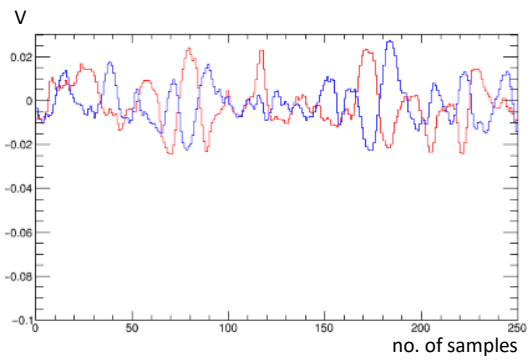

Output traces

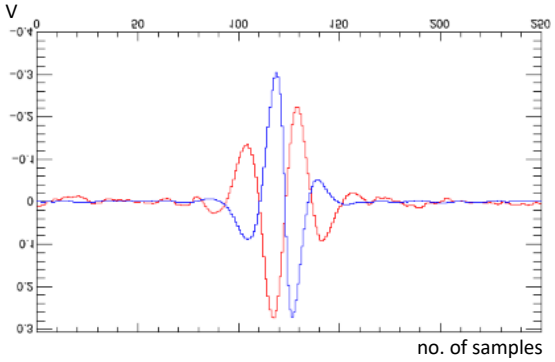

averaged and normalized traces

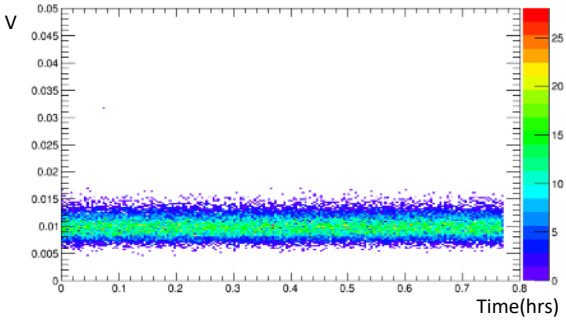

Noise level

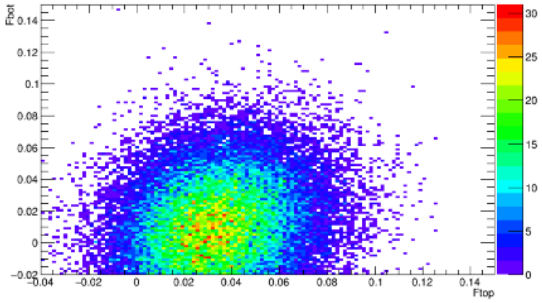

scatter plot

traces with foil between the boards and trigger on CosMo detector:

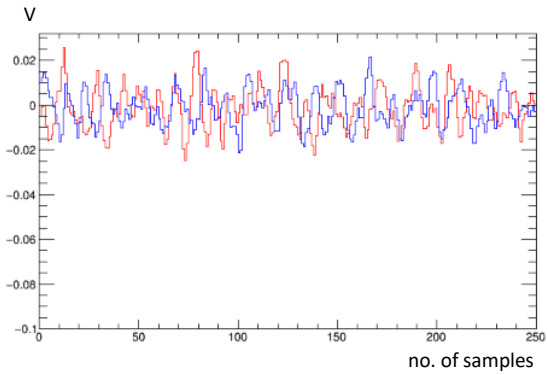

Output traces

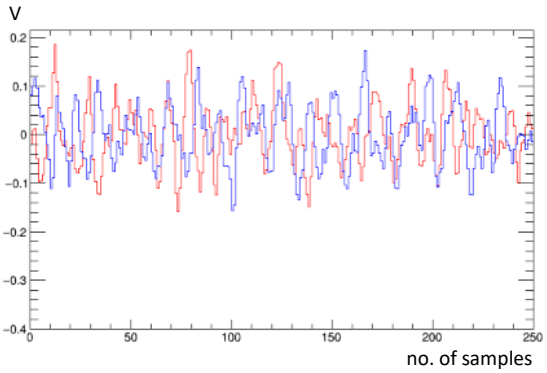

averaged and normalized traces

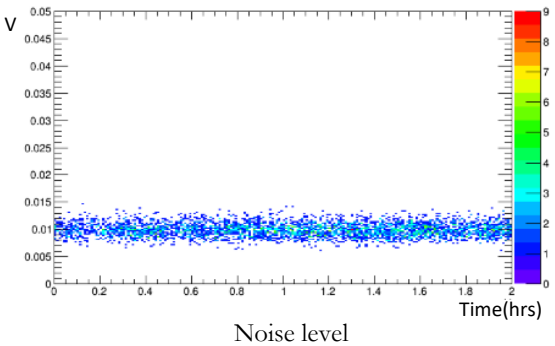

Noise level

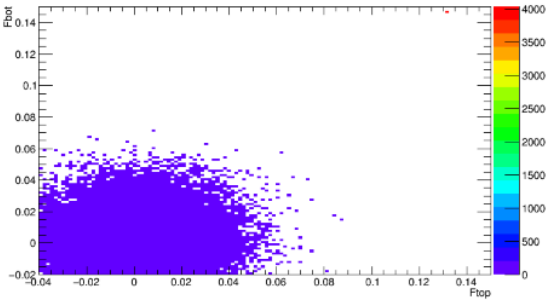

scatter plot

traces with trigger of 0mV on CosMO detector:

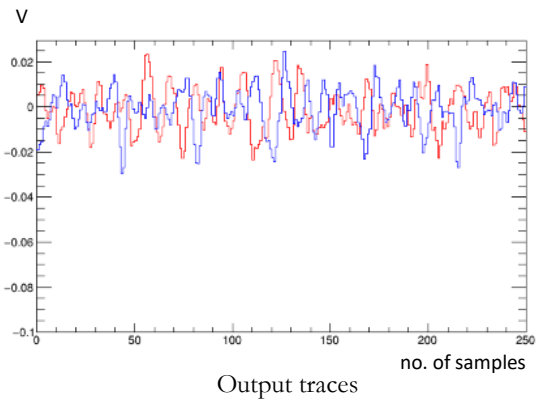

Output traces

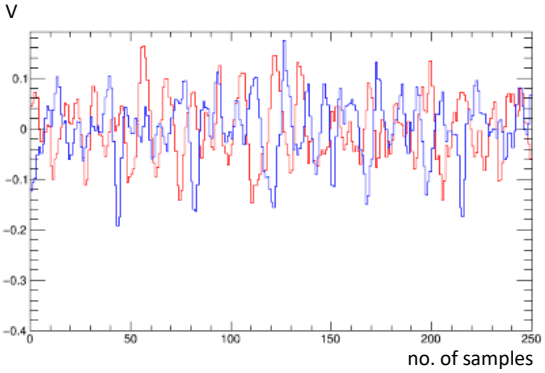

averaged and normalized traces

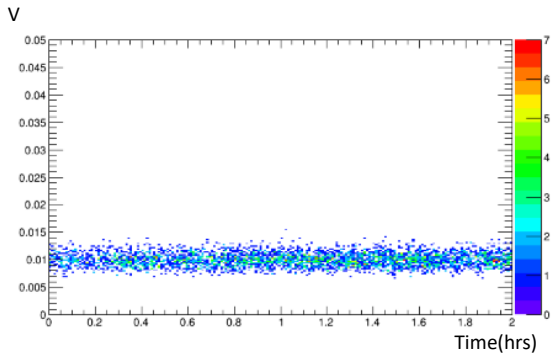

Noise level

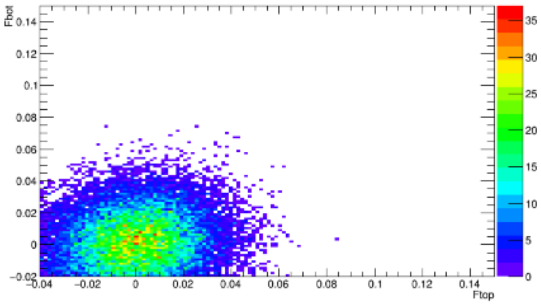

scatter plot

traces with the boards flipped with respect to each other and trigger set to a positive value on top board:

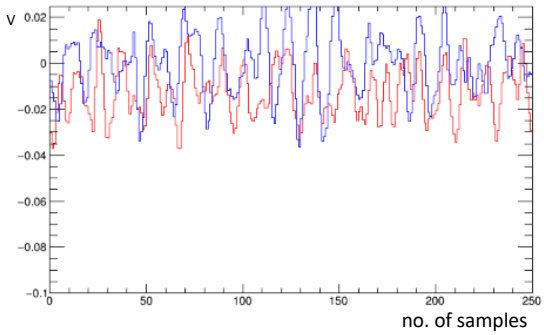

Output traces

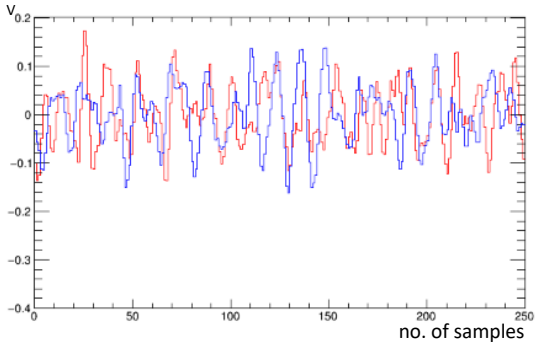

averaged and normalized traces

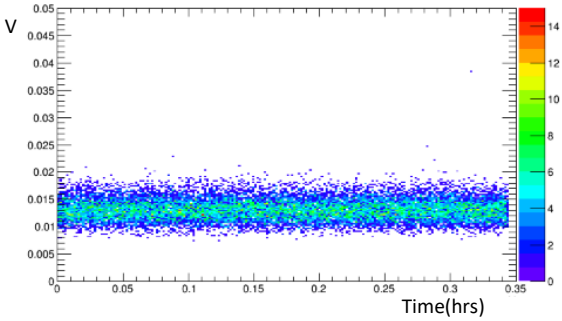

Noise level

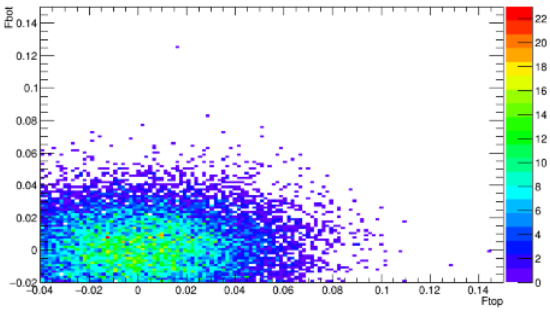

scatter plot

Program:

https://gist.github.com/Priyankakesav/8e83639bca75854f816510dc46b1a3a1